A Century of Technology Trends in Methanol Synthesis: any Need for Kinetics Refitting?

Filippo Bisotti[1], Matteo Fedeli[1], Kristiano Prifti[1], Andrea Galeazzi[1], Anna Dell'Angelo[1], Massimo Barbieri[2], Carlo Pirola[3], Giulia Bozzano[1], Flavio Manenti[1] *

[1] Dipartimento "Giulio Natta", Politecnico di Milano, Piazza Leonardo da Vinci 32, 20133, Milan (Italy)

[2] Politecnico di Milano, Technology Transfer Office (TTO), Piazza Leonardo da Vinci 32, 20133, Milan (Italy)

[3] Università degli Studi di Milano, Dipartimento di Chimica, Via Golgi, 19, 20133, Milan (Italy)

Corresponding author - * flavio.manenti@polimi.it

KEYWORDS

Methanol synthesis; CO_2 utilization, kinetics refit; robust regression; outlier detection; comparative example.

ABSTRACT

Recently methanol gained increasing attention thanks to the variety of feedstocks suitable for its production and its low environmental impact granting to the molecule a key role in future economic roadmaps as in Olah's development model. Nowadays, fossil sources are not the exclusive sources to produce syngas: biogas is a promising alternative leading to lies in less severe operating conditions and smaller plant scales. The most widespread kinetic models for methanol synthesis, namely Graaf and Vanden Bussche/Froment models, will be proven not to be fully adequate in characterizing these conditions. A robust refit is shown to outperform predictions from conventional models and follow recent trends in process operations. The refitted Graaf model is more flexible on the operating conditions and feed compositions, removing also some infeasible discontinuities present in conventional models. The final result is a more generalized and accurate Graaf's model for methanol synthesis on CZA catalyst.

INTRODUCTION

In 1905 Paul Sabatier and Jean-Baptiste Senderens were the first to synthesize and distillate under controlled conditions methanol on a copper catalyst. The research and interest in methanol synthesis intensively grew in few decades and the technological efforts led to the first industrial application in Leuna (Germany, 1923) licensed by BASF Company [1]. After a century from its first industrial plant, methanol is not only the key compound for the so-called methanol economy [2–8], but also a very promising molecule due to some key properties: (1) it can be produced from different feedstocks, not only fossil fuels (i.e. natural gas, coal gasification or naphtha), but also from alternative sources such as biomass, biochar and biogas; (2) it can be produced starting from CO_2, therefore, in principle, this is a possible chemical pathway to both reduce and capture emissions in the atmosphere and fix them into a new molecule [9]; (3) methanol is a bulk chemical with many applications and its market is wide and well-established; (4) methanol is a small molecule with a very high hydrogen-carbon ratio and for this reason it can be seen as an hydrogen carrier [9]; (5) it is a valuable synthesis intermediate to manufacture other chemicals such as dimethyl ether (DME) [10] and, finally, (6) methanol is a synthetic fuel suitable for internal combustion engines and it is already mixed with conventional fuels up to 20% v/v without modifications on the engine design [11].

Due to its key role in modern industrial chemistry, studies and research activities are driving the global synthesis of methanol towards higher bulk productions, while the operating conditions are becoming milder and milder. According to Sheldon [1], the global production of methanol (Figure 1~~Figure 1~~) increased by more than two orders of magnitude in half a century, from about 0.2 kt/d before 1970 up to about 25 kt/d before 2020. Despite the typical oscillations of bulk productions, mainly dictated by political, economic, and market fluctuations as well as the current energy transition outlook, the production is expected to grow another order of magnitude in the following 20 years.

On the other hand, the industrial operating conditions for methanol synthesis are seeing an opposite trend. Figure 2~~Figure 2~~ reports the variations of operative temperature and pressure typically adopted in industrial methanol plants during the last century. In 1923 in Leuna plant, the operating temperature was in the range of 300-400 °C, whereas the pressure was in the range of 250-300 atm. The current MegaMethanol technology by AirLiquide, for instance, operates at 250-260 °C

and 50-60 atm [12]. The detail of pressure conditions is shown in Figure 3~~Figure 3~~, where the semi-logarithmic representation emphasizes the technical and scientific progresses of the last century in enabling milder synthesis conditions. Roughly assuming that technological advances will progress at the same rate, it would be reasonable to expect that methanol will be synthesized at around 20-30 atm by 2050. This is not an unrealistic extrapolation when the number of filed patents per year in methanol synthesis is accounted; as shown in Figure 4~~Figure 4~~, with about 600 inventions per year in the last decade, against no more than 50 inventions per year before 1970, the process developments are more intensive now than ever. The dramatic reduction in the operating conditions (both temperature and pressure) occurred around 1959-1965 as depicted in Figure 3~~Figure 3~~ where it is possible to appreciate the pressure reduction below 100 atm. The catalyst formulation drove this outstanding improvement and disruptive technological achievement in the methanol production. The initial chromium-based catalyst used in Leuna plant (BASF technology) was improved initially by adding copper-oxide (patented by ICI in 1962). The methanol catalyst activity was furtherly improved removing the chromium amount leading to the final CZA catalyst [1]. Experimental works performed in the same period confirmed the higher catalytic activity of copper-based catalyst rather than chromium and mied copper/chromium catalysts [13]. The catalyst activity is still under investigation and recent publication demonstrate that there exist the potential for improving the catalyst formulation also in the perspective of CO_2 hydrogenation to methanol [14,15]. Deepening the analysis of new technologies and apparatuses (Figure 5~~Figure 5~~), it is worth noting that most of the innovations in the last three decades deal with the feedstock. This is mainly due to the change of raw materials used in syngas production, firstly from fossil to renewable sources and, then, to CO_2 for direct conversion. CO_2 as feedstock for bulk chemical processes is one of the greatest challenges that engineers are facing not only to make it functional [9,16,17], but also to reduce the energetic intensity of its capture [18–21] employing the guidelines provided during the Horizon 2020 program [22,23].

Either way, nowadays methanol is still mainly produced starting from fossil sources [24,25]. There are several chemical processes to convert fossil fuels into syngas and the rate of technological advances is speeding up also for this step (Figure 6~~Figure 6~~). Currently the most popular ones are Steam Methane Reforming (SMR) [26–28], AutoThermal Reforming (ATR) [25,29–31], Partial Oxidation (POX) [25,32] and Coal Gasification (CG) [33]. In past years, due to the large availability of coal mines, many institutions [34] devoted great efforts to making more appealing and environmentally sustainable CG

plants [5] mainly driven by the growth of the Chinese internal methanol market [35,36]. More recently, different strategies have been proposed to reduce the environmental impact of CG plants for methanol synthesis: the use of biomass from anaerobic digestion as an alternative feedstock [33,37–40] or the application of more innovative technologies to obtain syngas while purifying streams from common coal pollutants such as carbon dioxide [19] and H_2S (AG2S technology, [41–44]).

Although the largest amount of methanol is still produced starting from coal [45–47], the recent progress has been focusing on the incoming paradigm shift to atmospheric CO_2 as feedstock for methanol synthesis like described in in Olah's vision (Figure 7~~Figure 7~~). To support this transformation, the catalysis is constantly evolving. Figure 8~~Figure 8~~ shows the long tradition in patent filing in this field with the first iron-based and platinum-based catalysts dated as early as a century ago. Then, the Copper-Zinc-Alumina (CZA) catalysts appeared and subsequently the ruthenium-based catalysts up to the most recent Metal-Organic Framework (MOF) catalysts. Despite all the alternatives, CZA is not only the most used one in industrial synthesis catalyst but also the one with the largest perspectives as shown in Figure 8~~Figure 8~~.

Methanol synthesis is therefore moving towards larger bulk productions, lower operating conditions, new feedstocks, and new catalysts. **A key aspect that is not following suit with these technological trends is the kinetic modeling**.

The most common kinetic models in industrial practice are Graaf (GR) and Vanden Bussche – Froment (VBF). Their success lies in their simplicity and flexibility:

- few reactions are accounted;
- wide temperature and pressure ranges.

These models are well-established in scientific and industrial communities, but they are affected by some well-known shortcomings:

1. The original Graaf's model is suitable only for low to mid operating pressures while at P>50 bar it tends to underestimate methanol production;
2. VBF model is unable to manage a pure CO feed without steam (i.e. dry feedstock) and it properly works only at high pressure (P>50 bar).

This work proposes a model with a structure analogous to Graaf's, but with the kinetic parameters updated for higher prediction performance in the modern range of operating pressures. Some other

authors attempted a similar approach on both the GR and VBF models. Nestler and co-workers [48], for instance, removed dry-feed composition experimental data in their algorithm to avoid any numerical instability.

After an extended introduction, the paper focuses on technological trends in methanol synthesis in Section 2, theoretical background on the main works produced on methanol kinetics is provided in Section 3. Section 4 lists the experimental data for methanol synthesis on CZA catalyst used for the refit procedure, including recently published in-house data [49] for mild operating conditions. Section 5 is devoted to describing in detail the regression algorithm for model refitting including the techniques for robustness improvement. A quantitative comparison among Graaf, Vanden Bussche-Froment (VBF) and proposed refitted model is provided. Finally, further comparison for all the mentioned models has been done on an isothermal plug flow reactor implemented in Aspen HYSIS V10 using different feed compositions and pressures [50] showcasing the benefits of the refitted model.

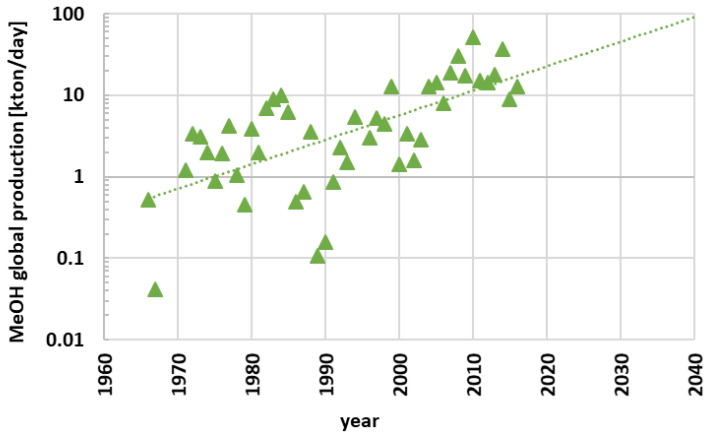

Figure 1 - Worldwide methanol production trend (rearranged from Sheldon [1]).

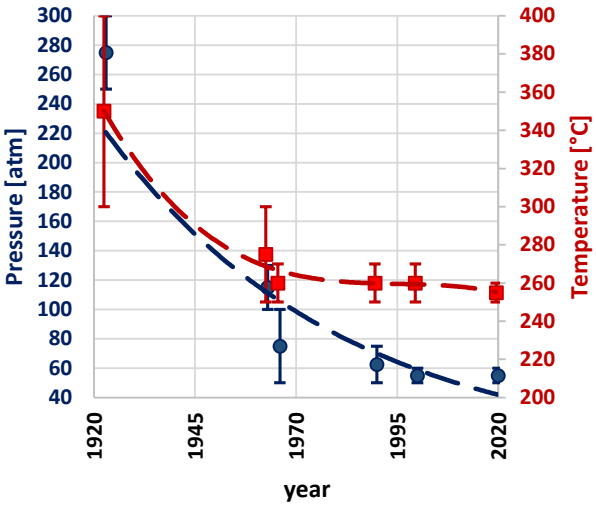

Figure 2 - Temperature and pressure trends in bulk methanol synthesis in the last century.

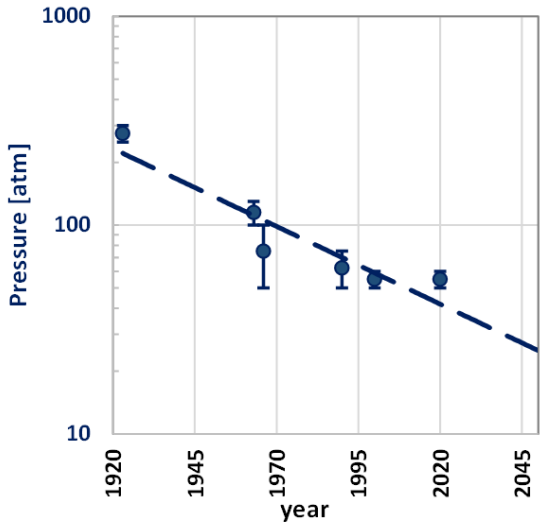

Figure 3 - Technological advances in one century research and development for pressure reduction.

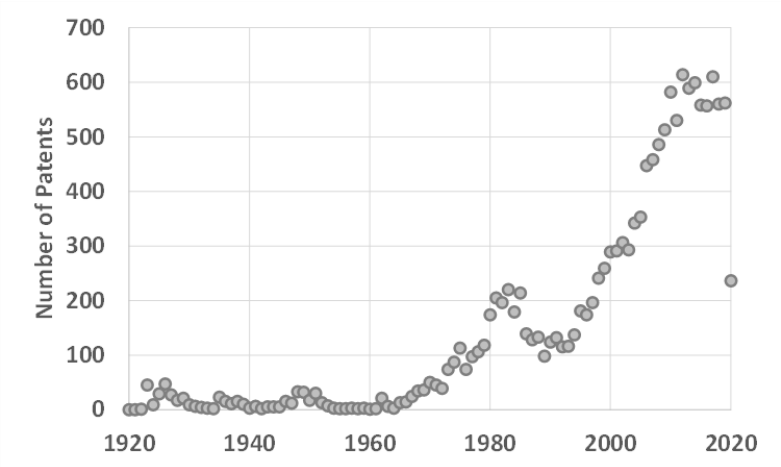

Figure 4 - Filed patents per year dealing with methanol synthesis. The datum for 2020 is only partial number, updated to March 2020.

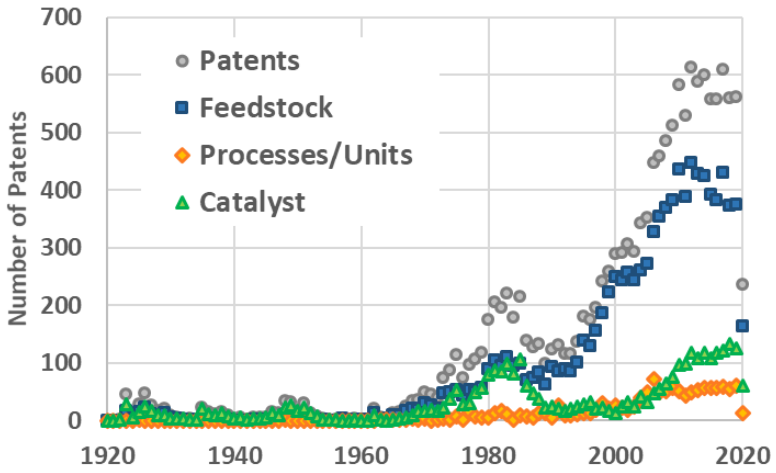

Figure 5 - Classes of patents filed for methanol synthesis: different feedstocks; different methods, apparatuses, and processes; different catalysts.

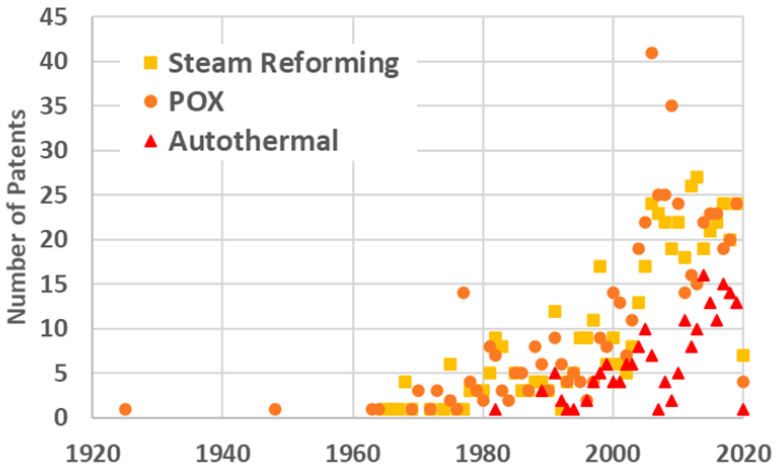

Figure 6 - Incidence of type of technology in the syngas-to-methanol class of filed patents.

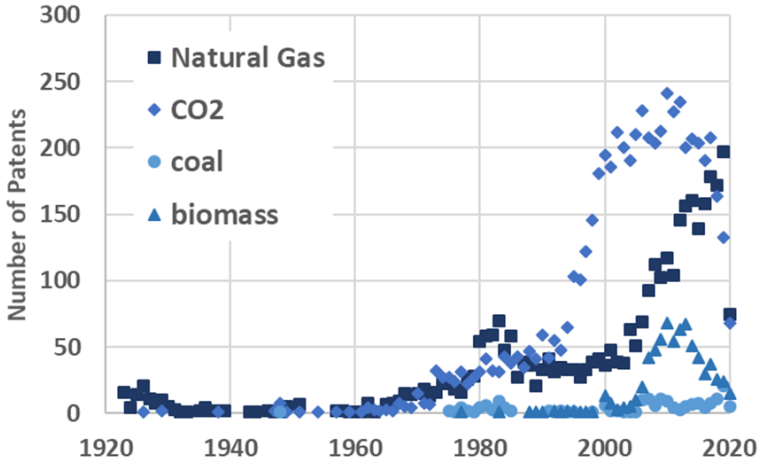

Figure 7 - Incidence of the source in the feedstock class of filed patents.

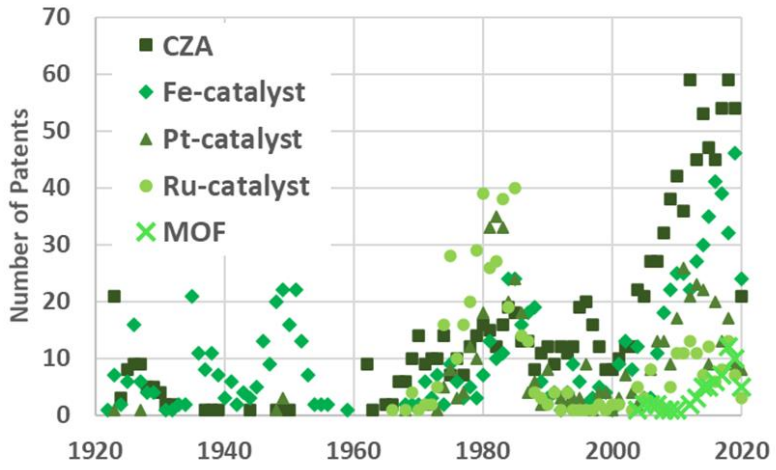

Figure 8 - Incidence of catalyst type in the catalyst class of filed patents.

TECHNOLOGY TRENDS

Patent filing and publication are realistic mirrors of the global market trends especially in the industrial sector, indeed, these allow to identify fields where, for instance, the chemical industry is projecting major efforts and economic interests in developing new technologies and/or improving the existing ones. In this work, the technological trends have been investigated through Orbit Intelligence (https://www.orbit.com - accessed on 3rd April 2021) a fee-based professional databased, and Espacenet (https://worldwide.espacenet.com - accessed on 1st April 2021) a free patent database. The search criteria and keywords used in the patents filing research is provided in the tables in Appendi C.

In 2018, the largest amount (66%) of worldwide methanol production was concentrated in Pacific Asia [51,52]. The second areas for methanol production are the Middle East which weights for 14% and North America 7% on the global methanol market. Europe production covers only 3% of the total. As in IEA reports, local raw material, as well as geopolitical concerns, determine the main locations of bulk chemicals production. Asia dominates both global primary production and naphtha consumption, however, coal satisfies part of the raw material consumptions (almost 24%). In addition, Pacific Asia is a unique macro area still using coal as feedstock, while Europe, Middle East, and North America consume naphtha and natural gas.

2522 patent families (inventions) have been identified for syngas-based methanol synthesis; 1084 are still active (granted or pending) and 649 have been filed in the period 2016 – 2020. The trend of filings is doubled in the last decade, as shown in Figure 9~~Figure 9~~. China, United States, and Japan are the three top priority and publication countries. 2503 patent families have been dedicated to CO_2 to methanol; 1256 are still active (granted or pending) and 380 have been filed in the period 2016 – 2020. Figure 7~~Figure 7~~ shows that the interest in CO_2 as feedstock is continuously growing since the 1960s and achieved a plateau in the 2000s (Figure 10~~Figure 10~~), the major publication countries are Japan and United States with a constant high rate of paper release.

Analogous interest is on CZA and iron-based catalysts. The CZA, the most use catalyst for methanol synthesis being described or claimed in 893 inventions, as depicted in Figure 11~~Figure 11~~. Iron-based catalysts are commonly used in industrial alcohols synthesis [53,54] and their costs, as for the CZA catalyst are lower compared to noble metals-based catalyst [55]. As already discussed in the previous paragraph the change in the catalyst formulation from chromium to copper-based catalyst (CZA) was the break point for the methanol synthesis at milder conditions. In the light of previous considerations on the methanol catalyst development, trends in Figure 5~~Figure 5~~ for catalyst patents is now clear. The first patent filing period was around 1920-1950, while the second peak is concentrated in 1960-1985 due to the renewed excitement for the new copper-based CZA catalyst. The third wave (starting from 2020s) contemplates the patents related to catalyst improvements for specific applications. A lower number of filed patents for noble metals-based catalysts reflects this consideration. More recently, MOFs are promising alternatives to conventional catalysts for methanol production [56–58]. This technology and the research in this field are still at an early stage as proven by few registered patents in the last five years.

Figure 12~~Figure 12~~ illustrates the impact of feedstocks on new technologies. It is noticeable the last 40 years were mainly dedicated to natural gas [25,32] and biomass-based technologies [59–61], whereas the coal technologies did not see the same progress. It is worth noting that the AutoThermal Reforming (ATR) counts less patents than the other technologies, which appear more consolidated. In any case, relevant players are recently giving growing attention to ATR [62,63]. On the other hand, in the last 5 years, the technological trends have changed. There is, in fact, a renewed interest in coal-based technologies with a similar number of patents if compared to biomass and natural gas-based technologies. This trend could be explained by readiness levels of carbon capture technologies able to make coal more environmentally sustainable [64–69]. It is possible to appreciate an increasing rate in patent filing and publications, indeed, almost 30% of all the patent filings of the last 40 years were submitted in the last lustrum. This trend is testimony

to the great excitement around the methanol sector and a renewed interest in improving the current technologies and introducing more efficient and sustainable processes driven by global energy transition [70].

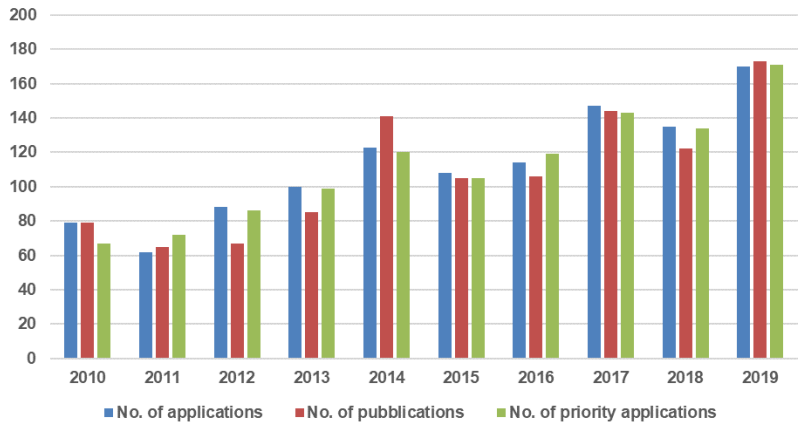

Figure 9 - Trend in filings and publications for the methanol synthesis inventions starting from syngas.

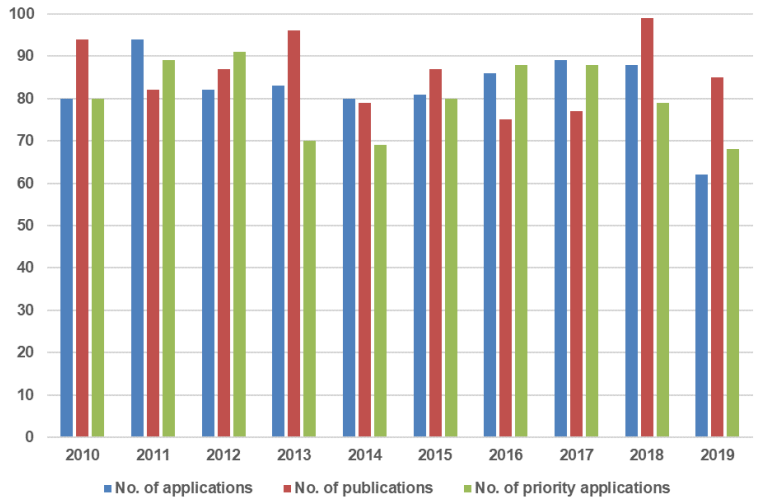

Figure 10 - Trend of filings and publication for methanol synthesis invention using CO_2.

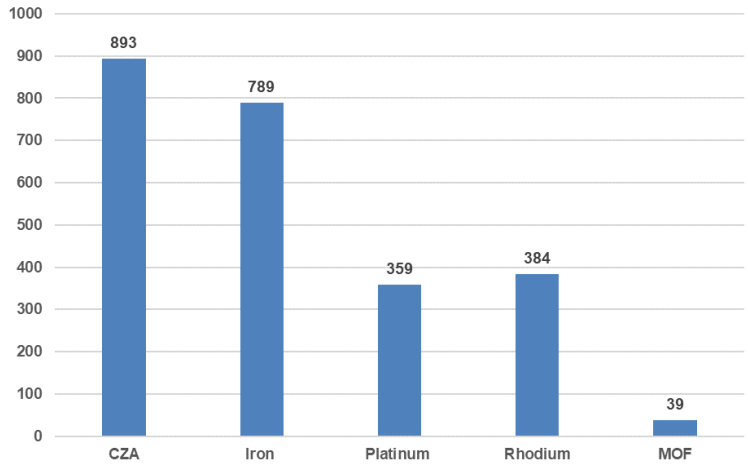

Figure 11 - Patents for conventional catalyst used in the methanol synthesis.

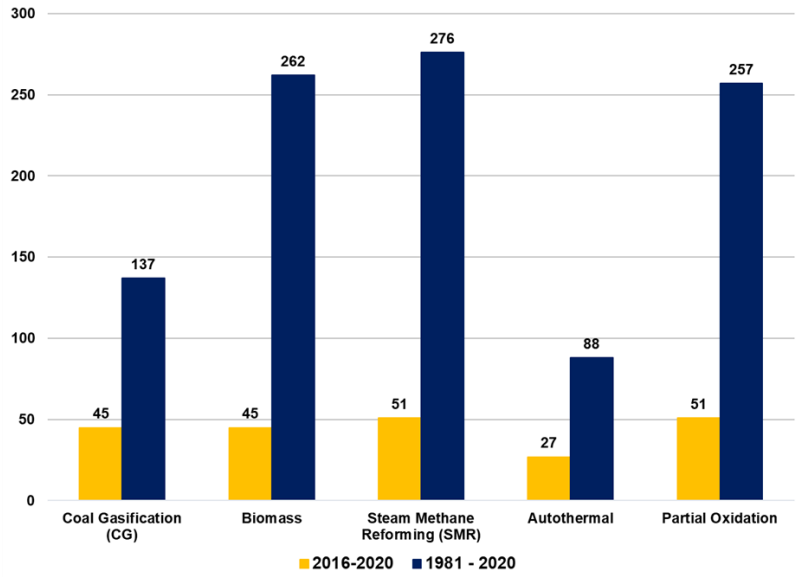

Figure 12 - Number of filed patents classified for sources of feedstocks. Natural Gas is represented by the summation of its three main technologies: Steam Methane Reforming (SMR), AutoThermal Reforming (ATR), and Partial Oxidation (POX).

THEORETICAL BACKGROUND

The most commonly used kinetic scheme for methanol synthesis via syngas (CO, CO_2, and H_2 with the variable relative ratio of the three components) consists of three main reactions [71,72]:

$$CO_2 + 3H_2 \leftrightarrow CH_3OH + H_2O \quad (1)$$

$$CO_2 + H_2 \leftrightarrow CO + H_2O \quad (2)$$

$$CO + 2H_2 \leftrightarrow CH_3OH \quad (3)$$

The mechanism to produce methanol starting from CO and CO_2 is not yet clearly understood. Historically, CO was considered the main carbon source for methanol production while CO_2 a stable component [73]. Later, the role of CO_2 as a reactant was introduced in kinetic models. Some authors state that the methanol reacting scheme is composed of only CO and CO_2 hydrogenations, i.e. reactions (1) and (3) [74–76], while others account also for their interchangeable roles through reverse water gas shift (RWGS), i.e. reaction (2) [77–81]. Others assume that CO_2 hydrogenation is

the only reaction pathway to produce methanol [82–85]. A summary of these four different kinetic mechanism proposals has been reported in Table 1~~Table 1~~ and a more detailed list is provided in review articles, such as Bozzano and Manenti [44]. The kinetic scheme could be complemented by side reactions, such as methanol dehydration to DME reaction or hydrocarbons formations, as reported in Park [80]. In the present study, these side reactions have not been considered because, due to their presence in traces, they were not always measured in the experimental data, thus, to make the dataset homogeneous these side products have been neglected.

Table 1 - Different carbon sources and kinetic schemes for methanol production

Authors	**Carbon source**	**Model Reactions**
Villa et al., 1985 [73]	CO	$CO + 2H_2 \leftrightarrow CH_3OH$ $CO + H_2O \leftrightarrow CO_2 + H_2$
Klier et al., 1982 [74] McNeil et al., 1989 [75] Ma et al., 2009 [76]	$CO + CO_2$	$CO_2 + 3H_2 \leftrightarrow CH_3OH + H_2O$ $CO + 2H_2 \leftrightarrow CH_3OH$
Takagawa et al., 1987 [78] Graaf et al., 1988 [77] Seidel et al., 2018 [79] Park et al., 2014 [80] Lim et al.,2009 [81]	$CO + CO_2$	$CO_2 + 3H_2 \leftrightarrow CH_3OH + H_2O$ $CO_2 + H_2 \leftrightarrow CO + H_2O$ $CO + 2H_2 \leftrightarrow CH_3OH$
Skrzypek et al., 1991 [85] Askgaard et al., 1995 [84] Kubota et al., 2001 [83] Vanden Bussche and Froment, 1996 [82]	CO_2	$CO_2 + 3H_2 \leftrightarrow CH_3OH + H_2O$ $CO_2 + H_2 \leftrightarrow CO + H_2O$

Since hydrogenation reactions are exothermic, an optimal temperature to balance kinetic and equilibrium is required. Currently, methanol synthesis is conducted in a multi-tubular packed-bed at moderate temperature (230-270°C) [71]. To favor the conversion of the reactants, high pressure

should be used. However, nowadays the processes are conducted in the range 50-100 bar to decrease the cost of gas compression [71,72].

The composition of the Synthesis gas fed to the methanol reactor can be characterized according to two parameters: the Stoichiometric Number (SN) and Carbon Oxides Ratio (COR) whose expressions are reported in (4) and (5).

$$SN = \frac{y_{H2} - y_{CO_2}}{y_{CO} + y_{CO_2}} \quad (4)$$

$$COR = \frac{y_{CO_2}}{y_{CO} + y_{CO_2}} \quad (5)$$

Where y is the molar fraction of the i compound.

A syngas with SN<2 indicates an excess of carbon oxides with the respect to H_2 and would lead to higher by-products formation [48]. When SN = 2 the reacting mixture is stoichiometric. Industrially, a syngas with slightly higher SN~2.05, i.e., so in excess of H_2, is used. The optimal value depends on the catalyst activity or the origin of the raw materials. In Løvik et al. [86] an optimal value of SN = 2.05 is reported, if the syngas comes from natural gas reforming a value of 2.8-3 can be achieved [44]. The optimal SN results in better catalyst performance, activity, and production rate. The COR defines the amounts of CO and CO_2 in the reacting mixture. In typical processes, COR is usually held below 0.6 [87] since higher amounts of CO_2 lead to drops in the reaction kinetics, equilibrium conversion as well as fast catalyst deactivation. However, in these conditions, the selectivity towards high carbon-content side products is lower [88]. The commercial catalysts are based on $Cu/ZnO/Al_2O_3$ (CZA catalyst) [49,89] where copper is essential to promote the shift reaction, changing the relative ratio among CO, CO_2, and H_2. The catalyst composition varies according to the producer, generally copper ranges in weight between 20% and 80%, zinc oxide from 15% up to 50% and Al_2O_3 content varies from 4% to 30% [90]. Additives and additional promoters, for instance, MgO, are present to decrease sintering resistance and increase the catalyst lifetime. CZA catalysts are active between 220 and 280°C and their selectivity to methanol reaches 99% [44]. Catalyst activity decreases due to deactivation by poisoning as well as thermal sintering. Typically, their average lifetime is about 4 years [44]. Many kinetic studies have been conducted to find the best kinetic rates for the model, but research is still ongoing for a definitive solution.

Microkinetic models, that also include adsorption interactions, can use as many as 50 reactions to describe the process as shown in several recent works [57,91,92]. The kinetic models industrially used for optimization and design of chemical reactors consider only the three reactions mentioned in reactions (1) – (3), or, in some cases, only two of them. In literature different models have been proposed, a comprehensive summary of them is reported and listed in Bozzano and Manenti review [44]. The most used are the kinetic models proposed by Graaf and Vanden Bussche-Froment (Table 2~~Table 2~~).

In this paper, Graaf model (GR) is assumed as more robust and complete since it accounts for both CO and CO_2 hydrogenation in presence of Reverse Water-Gas Shift (RWGS) reaction, which affects the CO_x relative ratio. This paper aims at improving the accuracy of Graaf model, through a nonlinear regression to refit its adaptative parameters (i.e., pre-exponential factors, activation energies, and adsorption heats). To accomplish this target, experimental data have been collected both from literature and further experimental campaigns [49]. These experimental data have been filtered through an outliers detection algorithm to remove gross errors which highly affect the regression performance. Through this step also internal consistency of the dataset was achieved by removing a limited number of experimental data which were overly impactful on the regression results.

Table 2 - Kinetic rate for Graaf and VBF models

Models	Reactions rates expressions
Graaf (GR) [77]	$r_{CO_2/MeOH} = \frac{k_1 K_{CO_2}\left(f_{CO_2} f_{H_2}^{\frac{3}{2}} - \frac{f_{MeOH} f_{H_2O}}{f_{H_2}^{\frac{3}{2}} K_{eqCO_2}}\right)}{(1 + K_{CO} f_{CO} + K_{CO_2} f_{CO_2})(f_{H_2}^{1/2} + (K_{H_2O}/K_{H_2}^{1/2}) f_{H_2O})}$
	$r_{RWGS} = \frac{k_2 K_{CO_2}\left(f_{CO_2} f_{H_2} - \frac{f_{H_2O} f_{CO}}{K_{eqRWGS}}\right)}{(1 + K_{CO} f_{CO} + K_{CO_2} f_{CO_2})(f_{H_2}^{1/2} + (K_{H_2O}/K_{H_2}^{1/2}) f_{H_2O})}$
	$r_{CO/MeOH} = \frac{k_3 K_{CO}\left(f_{CO} f_{H_2}^{\frac{3}{2}} - \frac{f_{MeOH}}{f_{H_2}^{\frac{1}{2}} K_{eqCO}}\right)}{(1 + K_{CO} f_{CO} + K_{CO_2} f_{CO_2})(f_{H_2}^{1/2} + (K_{H_2O}/K_{H_2}^{1/2}) f_{H_2O})}$
Vanden Bussche - Froment (VBF) [82]	$r_{CO_2/MeOH} = \frac{k_1 p_{CO_2} p_{H2}\left(1 - \frac{p_{MeOH} p_{H_2O}}{p_{H_2}^{3} p_{CO2} K_{eqCO_2}}\right)}{\left(1 + K_1 \frac{p_{H2O}}{p_{H2}} + \sqrt{K_2 p_{H2}} + K_3 p_{H_2O}\right)^3}$
	$r_{CO_2/MeOH} = \frac{k_2 p_{CO2}\left(1 - \frac{p_{CO} p_{H_2O}}{p_{H2} p_{CO2} K_{eqRWGS}}\right)}{(1 + K_1 \frac{p_{H2O}}{p_{H2}} + \sqrt{K_2 p_{H2}} + K_3 p_{H_2O})}$

COLLECTION OF EXPERIMENTAL DATASETS

The nonlinear regression analysis conducted within this study is based on several experimental data available in literature whose authors are listed in Table 3~~Table 3~~. Since most of the experimental data are available for high-pressure applications, to extend the dataset also at low-middle pressure, new experimental data available in Previtali et al. [49] has been included. Data has been clustered according to operative conditions (i.e., pressure, temperature, SN and COR). The collected observations (159 points, Appendix B) are suitable for performing a nonlinear regression

[93]. The new dataset covers the operative conditions relevant for both conventional methanol synthesis as well as low-middle pressure methanol synthesis via bio-syngas [94].

The selected dataset includes experiments conducted using a lab-scale PFR reactor with $Cu/ZnO/Al_2O_3$ as catalyst. Park et al. [80] report several experiments conducted at higher pressure (i.e. 50-80 bar) and temperatures ranging from 220°C up to 340 °C. Graaf [95] experiments were conducted at low pressure (i.e. 10-50 bar) with different temperatures and various inlet flowrates composition on CZA-based catalyst. We decided to limit the experimental data from Graaf's dataset and to consider only the experimental observations at 20 bar. This decision was made considering that Park provides a larger reliable dataset with a considerable number of observations around 50 bar. Consequently, we decided to add only Graaf's observations at 20 bar to balance the weight and number of the experimental observations (i.e., uniform distribution of experimental data over the pressure range of interest 20 - 60 bar). Otherwise, a huge number of experimental points close to 50 bar would have negatively impacted on the refit performance forcing the minimization solver to better predict close to 50 bar region by neglecting other portions of the investigation domain where observation were less dense [96,97]. As last consideration, we decided to limit the number of experimental data in the database not to reduce the computational time and efforts. We believe that 159 observations are sufficient to perform a kinetics refit. For these reasons, we considered the additional Graaf experimental points as redundant.

Table 3 - References for data set

Authors	Reference	Catalyst
Park et al., 2014	[80]	CZA Süd-Chemie MegaMax 700
Graaf, 1988	[95]	ICI 51-2 (CZA catalyst[77])
Previtali et al., 2020	[49]	CZA

APPARATUS FOR IN-HOUSE METHANOL SYNTHESIS EXPERIMENTAL DATA

The experimental bench-scale reactor used for methanol synthesis is described in detail in Previtali et al. [49] and briefly introduced here. 1 g of catalyst was loaded in packed bed configuration in a 6 mm diameter reactor with a length of 560 mm. Before the test, 20 $NmL \cdot min^{-1}$ of hydrogen was used to reduce in situ at 573 K, 0.8 MPa for 3 h the catalyst. Then, nitrogen (internal standard for chromatographic analyses), carbon monoxide, hydrogen, and carbon dioxide were mixed to the desired concentration as feed for the reactor. Reactants flow from the top to the bottom of the reactor with a GHSV of 4030 h^{-1}. A pressure controller regulated the pressure to a value of 2 MPa. An electrical furnace heated the reactor at the desired temperature. Before the pressure controller, a cold trap (T = 265 K) condenses methanol and water. A micro-GC (Agilent 3000A, carrier: He) samples the exiting gases every 1 h for the determination of the flow of exiting CO and, therefore, CO conversion. Moreover, the micro-GC detects the uncondensed methanol.

KINETIC PARAMETERS REFIT ALGORITHM

Kinetic parameters for the updated Graaf model have been refitted through a non-linear regression of the 159 experimental data points mentioned in the previous section.

Kinetic parameters in Graaf's model

For the parameters regression of the updated kinetic model, the Graaf reaction rate model has been chosen. Graaf's doctoral thesis and successive works [95] introduced the original parameters for Graaf model (Table 4~~Table 4~~). Thermodynamic equilibrium constants of the three reactions in the methanol synthesis are listed in Table 5~~Table 5~~ [49].

Table 4 - Original Graaf's kinetic parameters for low-pressure methanol synthesis as reported in Graaf's et al. work [98]

Reactions	Rates	Kinetic parameters
$CO_2 + 3H_2 \rightarrow CH_3OH + H_2O$	$r_{CO_2/MeOH} = \frac{k_1 K_{CO_2}\left(f_{CO_2} f_{H_2}^{\frac{3}{2}} - \frac{f_{MeOH} f_{H_2O}}{f_{H_2}^{\frac{3}{2}} K_{eqCO_2}}\right)}{DEN}$	$k_1 = 1.09 \cdot 10^5 \, e^{-\frac{87500}{RT}}$
$CO_2 + H_2 \rightarrow CO + H_2O$	$r_{RWGS} = \frac{k_2 K_{CO_2}\left(f_{CO_2} f_{H_2} - \frac{f_{H_2O} f_{CO}}{K_{eqRWGS}}\right)}{DEN}$	$k_2 = 9.64 \cdot 10^{11} \, e^{-\frac{152900}{RT}}$
$CO + 2H_2 \rightarrow CH_3OH$	$r_{CO/MeOH} = \frac{k_3 K_{CO}\left(f_{CO} f_{H_2}^{\frac{3}{2}} - \frac{f_{MeOH}}{f_{H_2}^{\frac{1}{2}} K_{eqCO}}\right)}{DEN}$	$k_3 = 4.89 \cdot 10^7 \, e^{-\frac{113000}{RT}}$
Adsorption constants		
$K_{CO_2} = 7.05 \cdot 10^{-7} \, e^{\frac{61700}{RT}}$		
$K_{CO} = 2.16 \cdot 10^{-5} \, e^{\frac{46800}{RT}}$		
$K_{H_2O/K_{H_2}^{1/2}} = 6.37 \cdot 10^{-9} \, e^{\frac{84000}{RT}}$		
where $DEN = (1 + K_{CO} f_{CO} + K_{CO_2} f_{CO_2})(f_{H_2}^{1/2} + (K_{H_2O}/K_{H_2}^{1/2}) f_{H_2O})$		

Table 5 - Equilibrium constants provided in successive Graaf's work [99]

Equilibrium constants expressions	
$\log_{10}(K_{eq,CO2}) = \frac{3066}{T} - 10.592$	$K_{eq,CO2}$ [bar^{-2}]; T [K]
$\log_{10}(K_{eq,RWGS}) = -\frac{2073}{T} - 2.029$	$K_{eq,RWGS}$ [-]; T [K]
$\log_{10}(K_{eq,CO}) = \frac{5139}{T} - 12.621$	$K_{eq,CO}$ [bar^{-2}]; T [K]

Reactor modelling

The reactor model is necessary to introduce component balances in the refitting procedure and build a correlation between input and output to interpret experimental observations. A simple one-dimension reactor model can be described using the following material balances over the axial direction z [80,100–102]:

$$\frac{dn_k}{dz} = \rho_b A_b \sum_{j=1}^{NR} \nu_{kj} r_j \qquad (6)$$

for each k-th component involved in j-th the reaction (reaction identification number as listed in Table 2~~Table 2~~ for Graaf's model). Since the reaction rates are defined as moles consumed in time per unit of mass of catalyst, the bulk density, i.e. mass of catalyst per global volume of the reactor, needs to be included in the calculations.

Regarding the energy balance, a constant axial temperature through the reactor has been considered due to the short length of the packed bed. Pressure drops have been neglected [48]. For the calculation of component fugacity, the Soave–Redlich–Kwong EoS has been considered in accordance to literature [48,103]. Finally, Graaf's experimental observations were obtained in a spinning basket reactor whose thermal behavior is similar to a CSTR. However, the PFR model was adopted in the light of the following considerations:

(1) In their recent publication, Nestler and coauthors [48] mentioned that that Graaf experimental apparatus is similar to a CSTR, however, they proposed only the PFR model to fit the experimental observations including the ones published in Graaf's works. Inspired by this recent publication, we decided to adopt a similar approach.
(2) looking at the experimental apparatus description and procedures [77], it is possible to state that the spinning basket reactor is likely a CSTR from a thermal point of view, meaning that the temperature is uniform within the reactor volume. However, bubble flows through a slurry where catalytic material is kept under agitation. Bubbles are progressively consumed thanks to the methanol synthesis occurring in the solid particles. Graaf demonstrated that his data were obtained under chemical regime. Bubbles arise along with the liquid volume, and they move through fictitious "channels" which are the space not

occupied by the solid particles. These channels make the bubble phase path closer to a PFR system. The combination of these two considerations convinced us to describe Graaf experimental system as a quasi-isothermal PFR

Moreover, it is important to observe that the PFR model coupled with the VBF kinetics is in good agreement with Graaf observations at 20 bar (Appendix B and Figure 17~~Figure 17~~). This last further consideration supports that the PFR modelling is anyhow a good approximation.

Optimization procedure

The most common algorithm is the ordinary Least Square (LS) method that minimizes the Euclidean norm of the residuals between experimental data and values provided by the model [104]. This method fails when the error is not normally distributed since it is strongly affected by either the presence of outliers or bimodal distributions. In these cases, a more robust approach should be applied. In several research papers [93,97,105,106] it has been proven that robust methods can detect outliers within a data set conversely to the LS method. Susanti [100] and Macchietto [107] provide different classes of robust estimation methods: M-estimation, S-estimation and MM-estimation. These procedures allow regressing adaptive parameters robustly and effectively such as in the case of kinetic laws (i.e. pre-exponential factors, activation energies, adsorption, and desorption equilibrium constants). The main advantages are reflected in a more stable convergence where parameters are less sensitive to perturbations caused by outliers [96,108,109]. As suggested in Hampel's work [110], robust regression can be combined with outliers detection.

The adopted stepwise procedure in this paper is sketched in Figure 13~~Figure 13~~:

1. LS method implementation
2. Curve fitting adopting M-estimator algorithm
3. Outliers identification and re-fitting on the reduced dataset

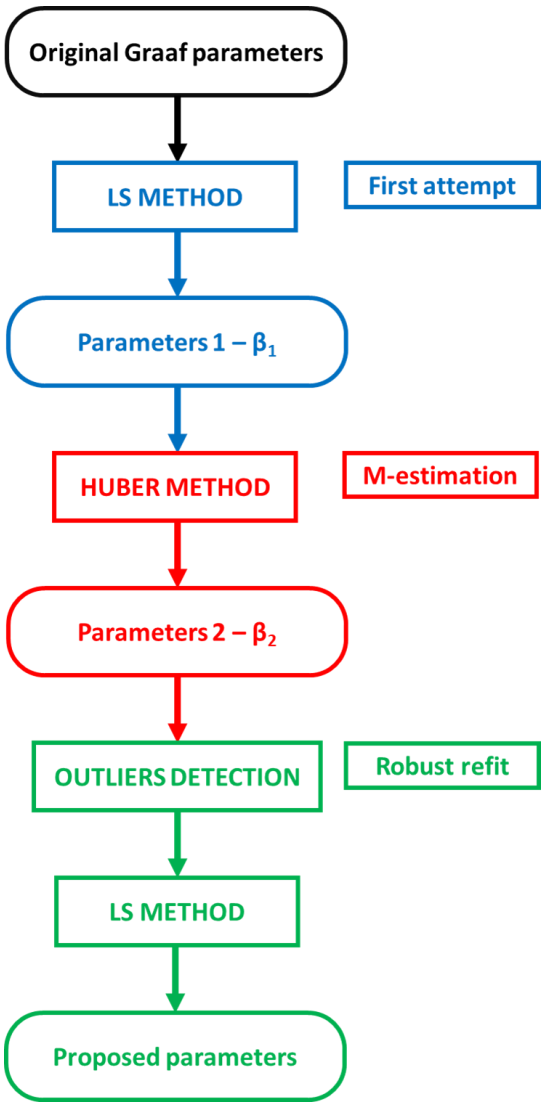

Figure 13 – Flowchart of stepwise procedure.

For the fitting procedure, the data has been imported to the reactor model described in the previous section. The nonlinear regression model has the form:

$$\hat{y}_i = f(x_i; \boldsymbol{\beta}) \quad i = 1, \ldots, n = 159 \tag{7}$$

where the model response $\hat{y}_i$ is related to the input variables x_i through the function f that depends on the constant parameter vector $\boldsymbol{\beta}$. The function is the component balance reported in Eq. (6). The residuals are calculated both for CO and CO_2 (CO_x), methanol and hydrogen output values as:

$$res_i = y_i - \hat{y}_i \tag{8}$$

where y_i is the i-th experimental point.

LS method

The LS method estimates the regression coefficients by minimizing the sum of squares of the residuals with the respect to vector $\boldsymbol{\beta}$ [111]. $\boldsymbol{\beta}$ vector contains the Degrees of Freedom (DoF) of the constrained optimization. The DoF of the minimization are:

- Pre-exponential factors appearing both in kinetic constants and adsorption parameters
- Adsorption activation energies
- Kinetic activation energies

$$\min_{\boldsymbol{\beta}} \sum_{i=1}^{n} \left(res_{i,CO}{}^2 + res_{i,CO_2}{}^2 + res_{i,MeOH}{}^2 + res_{i,H_2}{}^2\right) \tag{9}$$

$$\text{Subject to } v > 0$$

The sum has been minimized by adopting the original parameters of Graaf's model as first guess values (Table 4~~Table 4~~). The multidimensional, multimodal, constrained, and nonlinear algorithm has been implemented in MATLAB® 2019b setting as constraints (v in Eq.9) that adsorption and kinetic activation energies are non-negative entities. These variables are stored in vector $\boldsymbol{\beta}$.

The model outputs (i.e., the calculated outlet compositions $\hat{y}_i$), used in residuals estimates, comes from the solution of the differential material balances in Eq.(6). The initial conditions (feed compositions) are known from the experimental datasets and setup conditions described in

Formattato: Tipo di carattere: 12 pt

published works. The ODE solution takes advantage of the stiff system solver implemented in MATLAB® 2019b (ode15s). Hence, the numerical problem is a nested optimization, where the material balances (ODE) are integrated using kinetic parameters appearing in Graaf's model are iteratively manipulated by the optimizer. Optimization stops once minimum is reached.

Calculations have been performed on an Intel® Core™ i7-8700T: CPU (frequency 3.2 GHz), RAM 16.0 GB 2666 MHz (processor based on 64 bit). Computations required close to 10 hours.

The refitted parameters coming from the LS method have been used as first guess values in the procedure described in the following paragraph. At first, the estimated **β** vector is just a preliminary result that will be refined according to specific robust numerical analysis.

Robust method: application of M-estimator

β vector is refined by minimizing an assigned objective function ρ:

$$\min_{\boldsymbol{\beta}} \sum_{i=1}^{n} \rho(res_i) \quad \text{Subject to } v > 0 \tag{10}$$

where the function ρ, conversely to LS method, assigns different weights to each residual depending on the gap between the experimental observation and the model. In this way, the algorithm can filter part of the dataset according to the error. Therefore, residuals affected by large deviations will have a lower impact and influence on the regression algorithm [100]. Among the different objective functions belonging to the M-estimation class, the one proposed by Huber [93,112] has been selected for this study:

$$\rho_H(res_i) = \begin{cases} \frac{1}{2} res_i^2 & \text{for } |res_i| \le c \\ k\,|res_i| - \frac{1}{2}c^2 & \text{for } |res_i| > c \end{cases} \tag{11}$$

(12)

where c is a positive constant that can assume different values; in most cases, it is set equal to 1.345 [100]. The residual is divided by the standard deviation s [113] which is calculated as:

$$s = \frac{\mathrm{MAD}}{0.6745} \tag{13}$$

MAD is the median of absolute deviations of the residuals from their median and 0.6745 is a bias adjustment to make it consistent for the standard deviation under the normal distribution, as suggested in [100,113].

Outliers identification and final refit

Since experimental data may be affected by the presence of outliers and/or large errors, the dataset has been furtherly filtered according to the outliers identification procedure to remove them and robustly refitting the kinetic parameters. Once an outlier is detected, there exist different alternatives to handle its value as reported in some works on the topic [114,115]. It is possible to identify three different main approaches (others are slight modifications): (1) outliers removal, (2) data correction, and (3) keep the data and further analysis. In the proposed approach, we preferred removing outliers instead of correcting them. This choice was driven considering potential data heterogeneity in the dataset (hence, possible issues in estimate an accurate estimate for standard deviation and normalized value). Unfortunately, the dataset heterogeneity cannot be assessed a priori. To accomplish this final refinement, High Breakdown Diagnostics (HBD) has been applied [116]. The standardized residuals for both the fractions of CO and CO_2 have been calculated as reported in Eq.8. If the value of the standardized residual is higher than an assigned threshold value (i.e. 2.5 as suggested in Buzzi Ferraris [96]) the corresponding experimental case is detected as an outlier and a weight equal to zero has been assigned in the last LS estimation:

$$w_i = \begin{cases} w_i = 1 & \text{if } |res_i / s| \leq 2.5 \\ w_i = 0 & \text{otherwise} \end{cases} \tag{14}$$

(15)

The objective function of the last LS minimization becomes:

$$F_{obj} = \sum_{i=1}^{n} w_{i_{CO}} \left(res_{i_{CO}}\right)^2 + \sum_{i=1}^{n} w_{i_{CO_2}} \left(res_{i_{CO_2}}\right)^2 + \sum_{i=1}^{n} w_{i_{MeOH}} \left(res_{i_{MeOH}}\right)^2 + \sum_{i=1}^{n} w_{i_{H_2}} \left(res_{i_{H_2}}\right)^2 \tag{16}$$

The vector of parameters $\boldsymbol{\beta}$ obtained after this final step procedure is the one proposed for the model. Figure compares intermediate results and proves that the proposed updated Graaf-type model is more effective in predicting methanol synthesis as the stepwise optimization algorithm proceeds.

RESULTS AND DISCUSSION

Proposed kinetic model and comparison with the original Graaf's model

The kinetic parameters and adsorption constants resulting from the regression method are listed in Table 6~~Table 6~~. The comparison of parameter values is available in Appendix A.

Table 6 - Proposed refitted Graaf model parameters

Reactions	Rates	Kinetic parameters
$CO_2 + 3H_2 \rightarrow CH_3OH + H_2O$	$r_{CO_2/MeOH} = \frac{k_1 K_{CO_2}\left(f_{CO_2} f_{H_2}^{\frac{3}{2}} - \frac{f_{MeOH} f_{H_2O}}{f_{H_2}^{\frac{3}{2}} K_{eqCO_2}}\right)}{DEN}$	$k_1 = 9.205 \cdot 10^{1}\, e^{-\frac{45889}{RT}}$
$CO_2 + H_2 \rightarrow CO + H_2O$	$r_{RWGS} = \frac{k_2 K_{CO_2}\left(f_{CO_2} f_{H_2} - \frac{f_{H_2O} f_{CO}}{K_{eqRWGS}}\right)}{DEN}$	$k_2 = 4.241 \cdot 10^{13}\, e^{-\frac{149856}{RT}}$
$CO + 2H_2 \rightarrow CH_3OH$	$r_{CO/MeOH} = \frac{k_3 K_{CO}\left(f_{CO} f_{H_2}^{\frac{3}{2}} - \frac{f_{MeOH}}{f_{H_2}^{\frac{1}{2}} K_{eqCO}}\right)}{DEN}$	$k_3 = 2.240 \cdot 10^{7}\, e^{-\frac{106729}{RT}}$
Adsorption constants		
$K_{CO_2} = 1.540 \cdot 10^{-3}\, e^{\frac{14936}{RT}}$		
$K_{CO} = 8.206 \cdot 10^{-9}\, e^{\frac{76594}{RT}}$		
$K_{H_2O/K_{H_2}^{1/2}} = 3.818 \cdot 10^{-9}\, e^{\frac{97350}{RT}}$		
where $DEN = (1 + K_{CO} f_{CO} + K_{CO_2} f_{CO_2})(f_{H_2}^{1/2} + (K_{H_2O}/K_{H_2}^{1/2}) f_{H_2O})$		
Activation energies are expressed in [J/mol]		

Figure 14~~Figure 14~~ reports only the parity plots for CO_x and methanol comparison for experimental observations and model outputs using the reduced data set. The reduced dataset is the one obtained by removing detected outliers. For convenience, the authors report the chart of standardized residuals (Figure 15~~Figure 15~~) for experimental data which are listed in the same order as in Appendix B.

Table 7 - Comparison of activation energies in kinetic and heats adsorption constants

Parameter	Original Value [J/mol]	Refitted Value [J/mol]	Deviation Δ_E [%]
k_1	87500	45889	47.6
k_2	152900	149586	2.17
k_3	113000	106729	5.55
K_{CO_2}	61700	14936	65.8
K_{CO}	46800	76594	- 63.7
$K_{H_2O/K_{H_2}^{1/2}}$	84000	97350	- 15.9

In Table 7~~Table 7~~, both original and refitted activation energies and adsorption heats are listed and compared. From a preliminary comparison, it is noticeable that refitting procedure has kept the order of magnitude of each energy parameter. Moreover, the algorithm has deeply modified adsorption heats, while activation energies have been kept except for direct CO_2 hydrogenation, which is highly reduced. This last correction confirms what is depicted in Figure 14~~Figure 14~~b which shows original Graaf's model tends to underestimate methanol production. For this reason, the minimization algorithm tries to increase the methanol fraction in the product stream by acting on the production rate. Hence, CO_2 direct hydrogenation activation energy is drastically reduced. More in general, Figure 14~~Figure 14~~ clearly depicts the beneficial impact brought by the robust regression procedure in terms of accuracy both for CO_x (especially CO_2) and methanol formation prediction. For methanol, it is evident a strong alignment with the experimental observation and a drastic reduction of the original model inaccuracies.

The standardized residuals for both CO and CO_2 have been calculated and the ones crossing the threshold value of 2.5 have been identified as outliers. The standardized residuals are reported in Figure 15~~Figure 15~~. Globally, this study identifies 23 outliers (14.4% of the total amount of data) within the selected dataset.

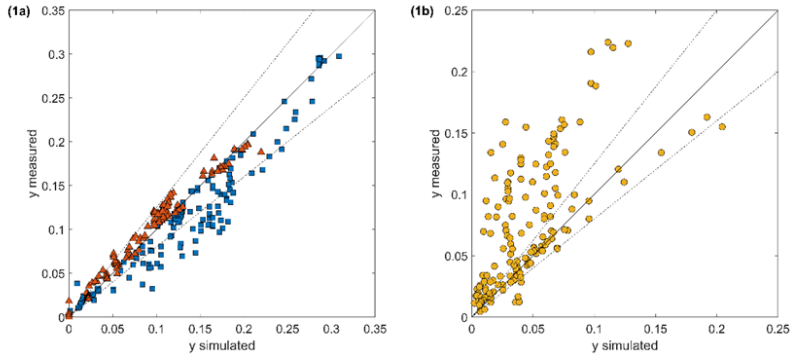

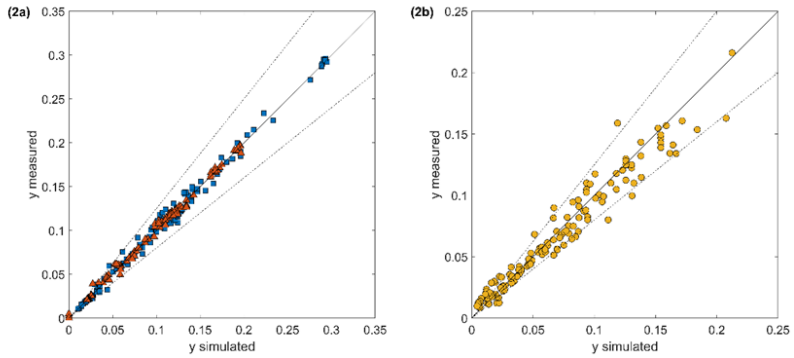

Figure 14 - Parity plots of molar fractions in products mixture: (a) CO_2 (blue square), CO (red triangle) and (b) methanol (yellow circle) for original Graaf (row 1) and refitted model (row 2)

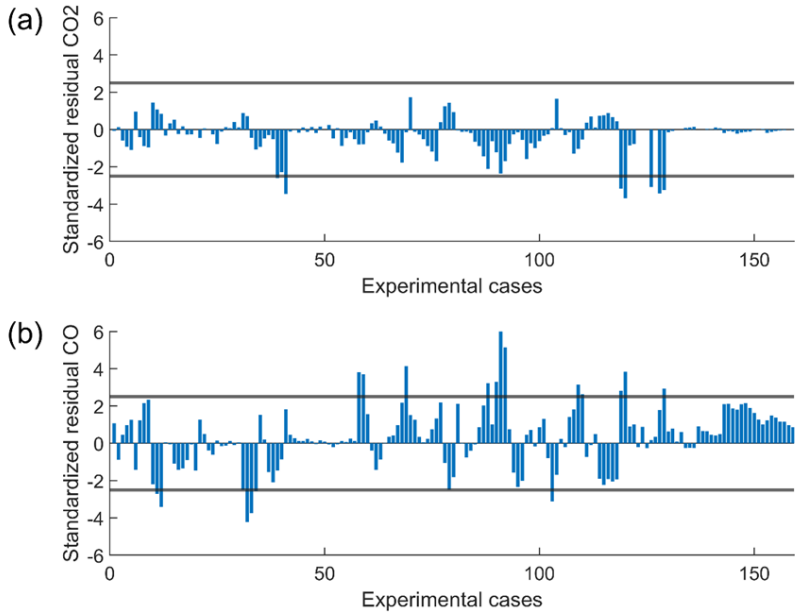

Figure 15 - Standardized CO_2 (a) and CO (b) residuals: horizontal lines are the threshold ±2.5.

Comparison with original Graaf and VBF models results

The refitted Graaf model has been compared to both the original Graaf [98] and Vanden Bussche and Froment [82] models. The comparison has been conducted analyzing the residual sum of squares and the ability of all the models to predict the measured values (the overall dataset, including the detected influential observations). The sum of squared residuals has been calculated on the overall dataset (Appendix B) for each model as:

$$\mathrm{Sum_{res}} = \sum_{i=1}^{n} (\mathrm{res}_{i,CO}^2 + \mathrm{res}_{i,CO_2}^2 + \mathrm{res}_{i,MeOH}^2 + \mathrm{res}_{i,H_2}^2) \quad (17)$$

The calculated residual sums are reported in Table 8~~Table 8~~.

Table 8 - Sum of square residuals for each model

Model	Sum_{res}	Sum_{COx}	Sum_{MeOH}	Sum_{H2}
Graaf (GR)	0.6760	0.1614	0.3632	0.1514
Vanden Bussche – Froment (VBF)	0.2175	0.0365	0.1124	0.0683
refitted Graaf	0.2030	0.0723	0.0483	0.0824

As it can be seen in Table 8~~Table 8~~, despite VBF kinetic model has the lowest value of the sum residual of CO_x, the Proposed Model better predicts the methanol production and the methanol content in the products mixture. As already discussed in Section 3, VBF model is unable to predict methanol formation without CO_2 and steam in the feed and it leads to significant spikes in methanol prediction error on those data points. The original Graaf model benefitted from the refit procedure: CO_x and methanol residual sum have been reduced by one order to magnitude, and specifically, more than halved (-54.3% and -86%), respectively. Original GR model presents the highest deviations from the experimental values, which means that: (1) original GR model may have not been filtered from outliers and/or gross errors and (2) it is not suitable to predict methanol synthesis at low-medium pressure. Consequently, the proposed model improves the GR model and solves some of its drawbacks such as being able to predict CO-to-methanol synthesis path also in mild pressure conditions, as happens in biogas conversion processes [117]. These considerations are seen in the sum of squared errors: the proposed model exhibits lower residuals with respect to GR and VBF models since the numerical procedure allowed to detect and remove outliers (i.e. robust refitting) for CZA catalyst also in presence of slight differences in the catalyst formulation and/or preparation.

As it can be seen in Table 8~~Table 8~~, the updated Graaf model presents the lowest sum of squared residuals. In details, the sum of the errors has been dropped up to less than one third of the original Graaf model. The refitted model is able to better spread on the CO_2, H_2 and MeOH compounds the deviation between the model predictions and the datasets; this allows to improve the general prediction with special focus on the methanol production.

The impact of the feed composition on reaction rates and carbon conversion has been investigated for the analyzed kinetic models. The feed is a mixture of CO, CO_2 and H_2, whose relative content

is the degree of freedom of the sensitivity analysis. The reactor is assumed isothermal (250°C) and the pressure fixed (50 bar) to test the model performance in modern mild industrial conditions as in the case of biogas-to-methanol small plants or more recent and innovative industrial methanol synthesis plants such as MegaMethanol. The Carbon Conversion defined in Eq.18 has been evaluated varying the COR value. COR ranges between 0 and 1, while the stoichiometric number (SN) has been set equal to 2, 2.2, and 1.8 to simulate different possible industrial feeds. Fixing SN and COR parameters the reactants mixture composition is properly defined.

$$X_C = \frac{\left[\left(n_{CO_2,in} + n_{CO,in}\right) - \left(n_{CO_2,out} + n_{CO,out}\right)\right]}{n_{CO_2,in} + n_{CO,in}} \quad (18)$$

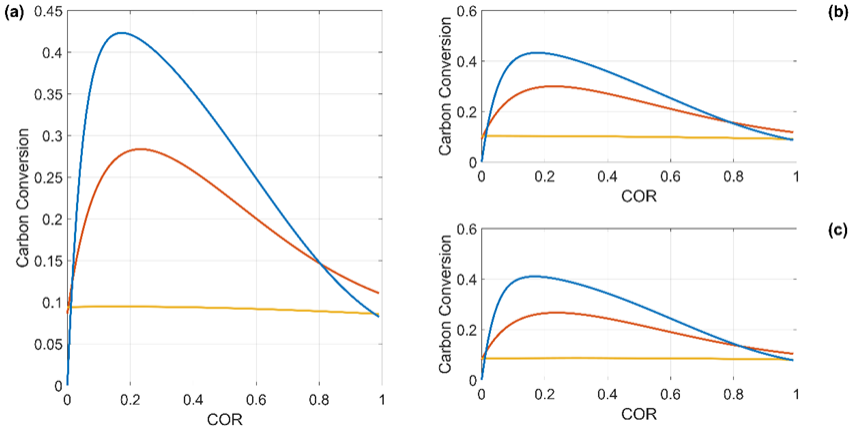

Figure 16 - Carbon conversion at different COR values: proposed model (red), GR (yellow) and VBF (blue) at fixed operating conditions T = 250°C, P = 50 bar: (a) SN = 2; (b) common industrial SN = 2.2; (c) SN = 1.8

Plotted profiles follow literature studies [48,118] (Figure 16~~Figure 16~~) and the refitted Graaf model preserves the general shape of the curve meaning that the refit procedure did not cause any unfeasible predictions or abnormal behaviors. In the calculations the refitted parameters have been used for the updated model (Table 6~~Table 6~~). Figure 16~~Figure 16~~ shows that all the kinetic models

reach a maximum of carbon conversion at low values of COR (small content of CO_2): there are slight differences between the models' sensitivity toward COR. Despite peaks are present for similar values of COR, the amplitude of the maximum peak is considerably different: the original Graaf model shows a flat profile, while the proposed model tends to replicate the VBF profile. Focusing on Figure 16~~Figure 16~~(a), the VBF model shows a peak in carbon conversion at COR equal to 0.17 predicting a global carbon conversion of 43% while the refitted model reaches a maximum around 28% for COR close to 0.23. The chart also points out the low activity of Graaf kinetic model whose conversion does not overcome 10%, while VBF predicts a larger methanol production. The trend of the proposed kinetic model is comparable to VBF model: the proposed refit is a trade-off between the original model and VBF till COR around 0.8. After this point, the proposed model overcomes the VBF Carbon Conversion. However, the discrepancy in the predicted carbon conversion is limited (20%). Analogous considerations can be provided for lower and higher SN as depicted in Figure 16~~Figure 16~~ (b) and (c) cases.

Finally, predictions for the methanol production for the three kinetic models have been investigated and compared to the experimental observations (Appendix B) where detected outliers are included. Figure 17~~Figure 17~~ depicts the relative errors among predicted methanol production and experimental data. Horizontal thick lines confine the ±25% deviation space. According to the chart, it is possible to state:

(1) Limited to our analysis and the provided results, VBF model under certain conditions tends to overestimate the real activity of the catalyst whereas Graaf model tends to underestimate methanol production. These models exhibit large deviations in some points inside the domain of industrial interest. The exploitation of heterogenous datasets (slight catalyst formulation and corresponding different catalytic activity at mild or high pressure) may lead to this conclusion. However, the experimental observations have been selected considering similar catalysts. Hence, systematic errors in pressure-activity relations should be limited. The absence of systematic errors in pressire-activity is furtherly confirmed in the next paragraph (Figure 18~~Figure 18~~ - Figure 22~~Figure 22~~) where charts shows smooth profiles meaning that abnormal trend associated with systematic errors are not present. In conclusion, we would remark that this work aims at finding a more accurate and general Graaf kinetic model to describe the methanol synthesis over CZA-based catalysts even for different

catalyst formulation. We were convinced in pursuing this target once we realized that Graaf model is reliable only for $20 < P < 50$ bar. Hence, to achieve this target, we are forced to collect experimental observations coming from different (hence potentially heterogenous) experimental campaigns. Currently, in the literature there are not works dealing with the catalyst performance over a wide pressure range. Researchers preferred focusing only on a narrow pressure range (i.e., middle-low pressure 30 - 50 bar or high pressure, $P > 50$ bar). The generality purpose requires that we need to accept to use these data from different CZA catalyst (even in presence of slight catalyst formulation) at different operating conditions knowing that this may cause potential systematic errors in the pressure activity relations which have not been detected in the present work.

(2) Original Graaf model suffers from high-pressure domain (i.e. $P>50$ bar) since it was developed for milder operative conditions. In any case, it manifests large deviations also for experimental points within its applicability region. This might be due to Graaf and co-workers not removing influential observations from their experimental points which highly affected the numerical fitting;

(3) Proposed model predictions concerning methanol production mostly stay between the values provided by the other two and, more in general, in large part of the sample, the relative error is included within ±25%;

(4) In the case of pure CO feed, the VBF model is unable to predict methanol production since it considers only the direct CO_2 hydrogenation pathway. Conversely, the proposed model can operate in presence of pure syngas (i.e. only CO and H_2 feed composition). This aspect was also pointed out by Nestler et al. [48]; however, they did not prefer to furtherly investigate and solve this issue related to VBF model;

To further increase refitted GR accuracy, Park's experimental data [80,81] have been also considered to extend operating conditions not only in terms of temperature and pressure but also feed composition, including dry feed that VBF model is unable to handle even though some authors in this condition either preferred to add fictitious traces (100 ppm) of carbon dioxide to activate VBF mechanism to enable kinetic model parameters refit [103] avoiding any numerical instabilities or directly removing experimental data acquired under such conditions [48]

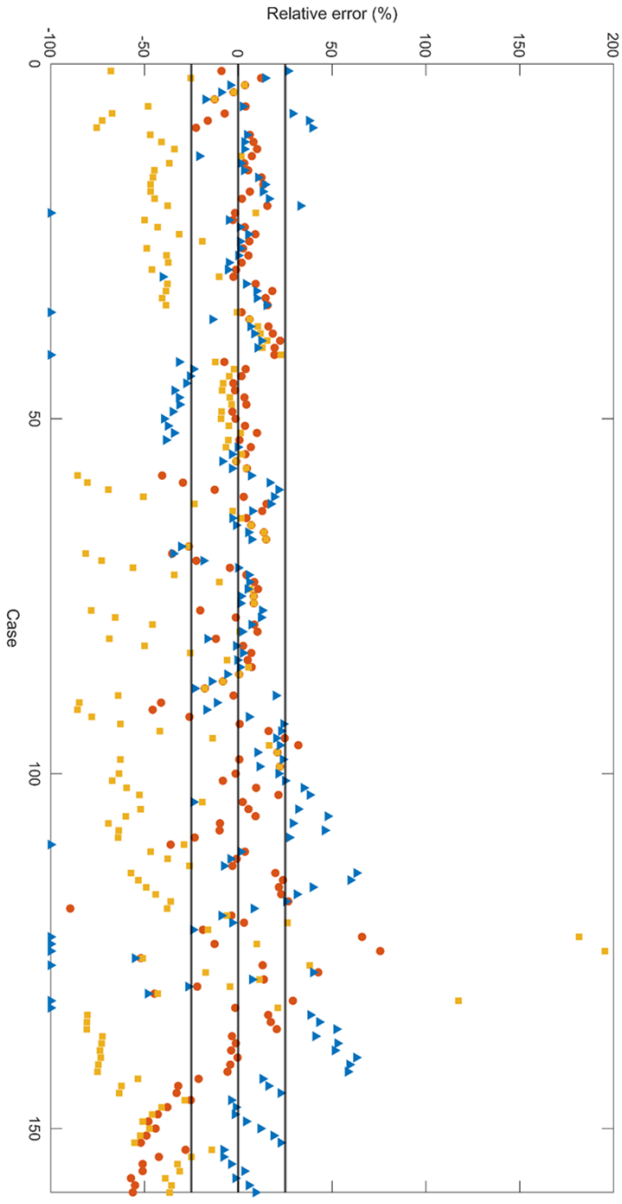

Figure 17 - Relative errors in methanol production flowrates according to: proposed refitted model (red cycles), Graaf (yellow square) and Vanden Bussche – Froment (blue triangle).

Kinetic models comparison at the process scale (bio-methanol plant)

Finally, the refitted Graaf kinetic model has been implemented in Aspen HYSYS V.10 to compare methanol productivity and the conversion of reactants (CO_2, CO, H_2) with regards to the original Graaf kinetic model and VBF at different operating conditions (pressure and syngas feedstocks and composition). The simulation flowsheet consists of an isothermal plug flow reactor for biomethanol synthesis. Reactor data and pressure range are reported in Table 9~~Table 9~~; while feedstock compositions are reproduced from Leonzio's paper [50] and listed in Table 10~~Table 10~~.This further analysis allows to implement the proposed refitted Graaf model in the process simulator to obtain reliable and instant material differential equation integration. The simplified flowsheet permits to focus the attention only on the conversion of reactants and methanol productivity per single pass in a PFR reactor, hence, without considering the complete methanol synthesis scheme and the impact of the recycle loop.

Table 9 - Reactor data

Variables	Values	UOM
Tube Length	4.00	m
Inner diameter	3.81	cm
Tubes number	25	-
Void Fraction	0.40	-
Feed Flowrate	50.00	kmol/h
Pressure Ranges	30-80	bara
Reactor Temperature	250	°C

Table 10 - Analyzed feed compositions (molar fraction or ppm)

Specie	Petro-Syngas	Syngas	Flue Gas	Coke Oven Gas	Bio-Syngas
H_2	0.6087	0.8000	0.803	0.4800	0.6504
CO	0.0795	0.0476	0.017	0.4160	0.2519
CO_2	0.0842	0.0295	0.173	0.0370	0.0856
H_2O	600 ppm	600 ppm	1000 ppm	-	700 ppm
CH_4	0.2183	0.1192	-	0.0220	0.0114
CH_3OH	2400 ppm	3000 ppm	5000 ppm	-	-
N_2	6300 ppm	100 ppm	-	0.0300	-
O_2	-	-	-	6000 ppm	-
H_2/CO	7.66	16.81	47.24	1.15	2.58
CO/CO_2	0.95	1.61	0.10	11.24	2.94
SN	3.20	10.00	3.30	0.98	1.67

Results have been obtained for isothermal reactor changing the operating pressure and they are graphically provided in Figure 18~~Figure 18~~ - 22. For each feedstock, four plots have been generated: methanol (a). Further charts are CO_2 (b), CO (c), and H_2 (d) conversions, respectively.

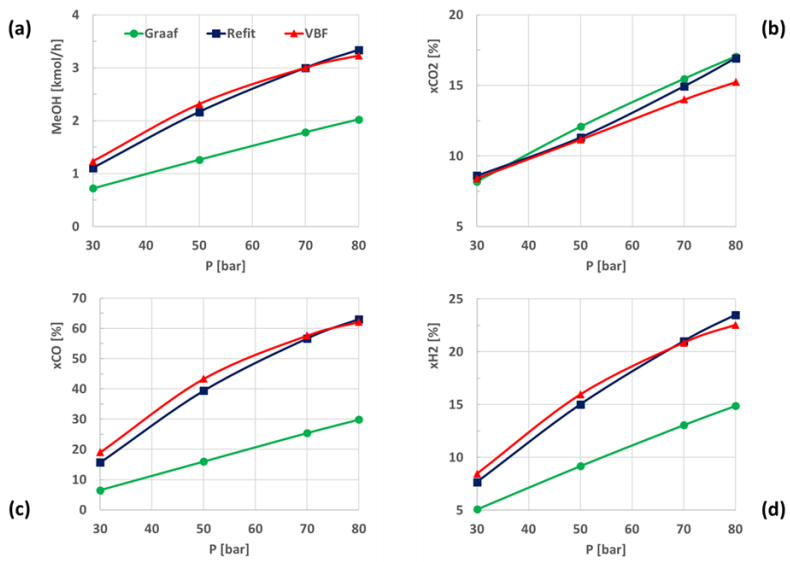

Figure 18 - Petro-syngas methanol production and conversion plots

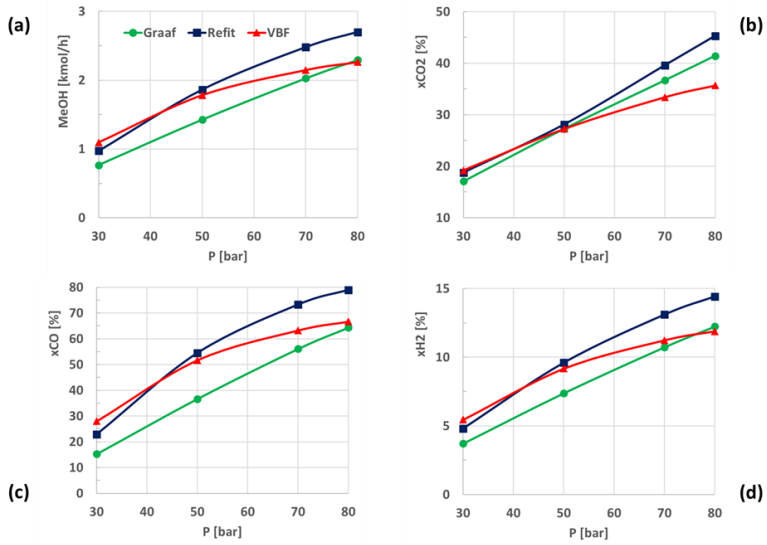

Figure 19 – Syngas methanol production and conversion plots

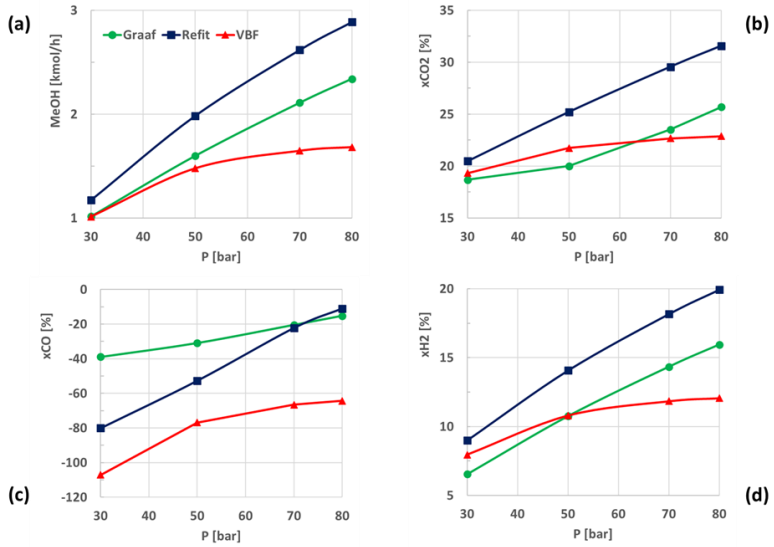

Figure 20 - Flue gas methanol production and conversion plots

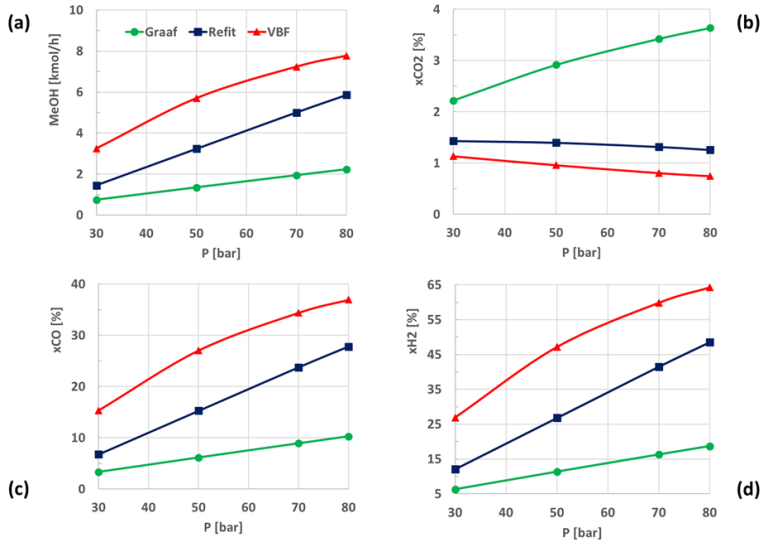

Figure 21 - Coke Oven Gas (COG) methanol production and conversion plots

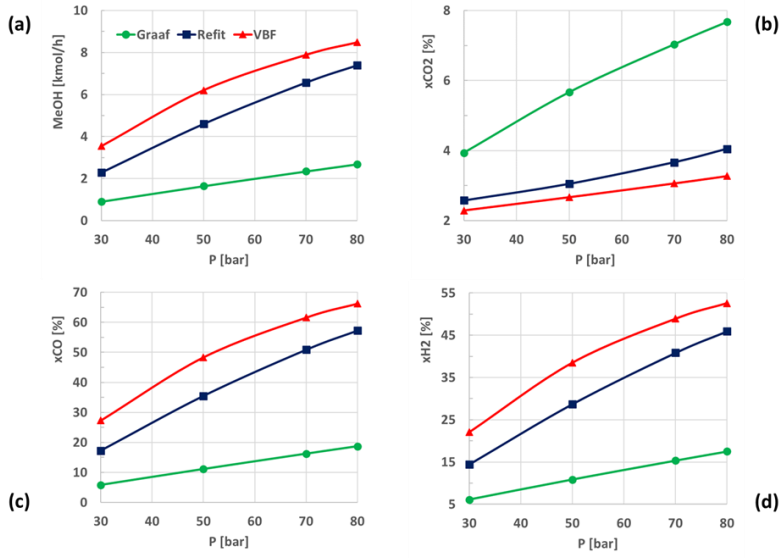

Figure 22 – Bio-syngas methanol production and conversion plots

Figure 18~~Figure 18~~ (Petro-gas) and Figure 19~~Figure 19~~ (syngas) depict that refitted kinetic model overlaps the VBF profile for methanol productivity and CO and H_2 conversion at fixed pressure, whereas for the CO_2 conversion predictions are very similar for all the analysed kinetics. Moreover, concerning the syngas feedstock (Figure 19~~Figure 19~~), the refitted model shows a positive discrepancy (+10%) in methanol production for pressure larger than 50 bar, and this is also reflected in the CO_x conversion meaning that both CO_2 and CO direct hydrogenation pathways are active in methanol production. These two feedstocks are characterized by a large excess of H_2 and small CO_x content. In the light of the GR and VBF kinetic schemes it is possible to justify the gap in the overall methanol productivity: on the catalyst surface, the RWGS takes place with the production of CO, which is directly hydrogenated to methanol in Graaf's scheme while, according to VBF mechanism, CO_2 direct hydrogenation is favoured for large hydrogen partial pressure and RWGS works in parallel until shifting reaches the equilibrium. As highlighted in Park et al. [80], there is not yet full clarity on the CO or CO_2 prevalent path for methanol synthesis.

Different trends are obtained for the flue gas feedstock (Figure 20~~Figure 20~~), which contains a significant amount of CO_2 (17% mol/mol). In this case, the direction of WGS is shifted towards the reverse path and this is reflected in significant production of CO (i.e. negative conversion of CO). Conversely to Graaf, VBF model predicts the highest value due to fact that the kinetic scheme does not consider the direct CO hydrogenation resulting in continuous production and accumulation of this species. This is compliant with what was observed also in Leonzio [50]. For this CO_2-rich feed, refitted kinetic model shows positive deviation in CO_2, H_2 conversion and methanol productivity (~70%). As already discussed in the refitting procedure section (Table 7~~Table 7~~), regression method provides a lower CO_2 hydrogenation activation energy. This means that CO_2-to-methanol kinetics are more active, hence, higher CO_2 conversions are expected for the refitted model compared to the original Graaf.

Finally, the profiles for COG (Figure 21~~Figure 21~~) and bio-syngas (Figure 22~~Figure 22~~) are very similar: in these cases, the refitted kinetic lies between VBF and GR. These two feedstocks have a similar CO and H_2 contents with a small amount of CO_2 (i.e. low COR). In these cases, the direct WGS is active and not the reverse path, hence, CO_2 direct hydrogenation is likely the main chemical mechanism to produce methanol. As already discussed, the refitted model enables a more active CO_2 direct hydrogenation to methanol, and this justifies the gap between original Graaf's model and refitted one. Indeed, the refitted model profiles are closer to the VBF's results.

More in general, process simulation results highlight more flexibility of the refitted kinetic models relating to different feedstocks, this model manages the shortcomings of VBF and GR respecting the chemical pathways of the reactions, this is clear from the profile curves. Indeed, the refit procedure heavily impacted the CO_2 direct hydrogenation: the gap reduction between VBF and original Graaf is partially due to the refit procedure which corrected kinetic parameters moving the refitted model closer to the VBF curve. In other words, as shown in methanol production from syngas (both petro- and bio-) and COG, the refitted model predictions are very similar to VBF model except for feedstock with large content in CO_2. At such operating condition, RWGS affects the CO_2/CO ratio, and this impact is reflected in:

(1) CO hydrogenation becomes the preferential chemical path to methanol production, and hydrogen partial pressure progressively reduces owing to RWGS and CO hydrogenation;

(2) CO is accumulated in the system, as also show in [50], however, differently from Graaf scheme, VBF model is not able to convert it into methanol.

For these reasons, refitted model predicts larger methanol production rather than VBF one in systems with large excess of CO_2. In almost all the other analysed feedstocks, the discrepancies between VBF and refitted model are slight, and, in some cases, there is an overlapping.

However, on industrial scale it is common practice to feed methanol reactors with syngas close to stoichiometric condition (optimal SN is 2.05 as investigated by Løvik and co-workers [86]) and excess of H_2 ($2<H_2/CO<3$) with variable amount of CO_2 (i.e. variable COR) [87] according to the installed syngas generation technology. This means that the most common case in an industrial plant is represented by biosyngas and petro-syngas feedstocks as reported in the literature case studies [101,119,120] and real methanol industrial plants data [30,31]. However, CO_2/H_2 mixtures as feedstocks for methanol synthesis are under investigation and they becoming more and more appealing for sustainability and environmental impact reasons [55,121–124] despite Carbon Capture Utilization and Sequestration (CCUS) still represents a relevant cost item in industrial plants as recently reported by the IEA [70].

Following from these considerations, Figure 23~~Figure 23~~ depicts the reaction rates for CO_2 and CO hydrogenations, and RWGS using bio-syngas as feedstock. Since VBF's model does not consider CO-to-methanol reaction, this reaction profile is missing in the corresponding charts. Once again it must be stressed that refit procedure has partially modified the original Graaf's model pushing this one towards the VBF model's profiles. This is clearly detectable in RWGS and CO_2 direct hydrogenation rates profiles. For the first case the minimum trends are present also for the refit model whereas original Graaf model shows a decreasing linear profile. Moreover, according to VBF and refit model, the RWGS reaction is always shifted favouring CO_2 and H_2 production. Conversely, original Graaf's model predict a completely different reactor behaviour: RWGS is effectively active in the first halve catalytic bed (i.e. equilibrium favours CO and steam production), while, an opposite trend is registered in the last part of the tubes where reaction rate becomes negative. Looking at CO_2 hydrogenation rates, it is remarkable that proposed model tends to predict larger reaction rates and the shape profile along the reactor is more like the one provided by VBF's kinetics. The reaction rates for CO_2 and CO consumptions are very different: the original Graaf model shows a flat profile and reaction rates values, at least, are by one order of magnitude

lower meaning that this chemical path is not the preferential way to synthesize methanol. The flat profile is repeated also for increasing pressure; hence, CO_2 direct hydrogenation is not even influenced by the pressure. In Graaf's model CO-to-methanol is the main active chemical path. This last consideration is confirmed by reaction rates for the CO hydrogenation, where the refitted rates always lie below the original Graaf's curves. In addition, the proposed model predicts that CO_2 consumption rate is at least ten times the corresponding CO consumption reaction. Hence, the conclusion is that the proposed model still preserves the direct hydrogenation of CO as a feasible kinetic mechanism to produce methanol, however, it enables to also hydrogenate the CO_2, while RGWS is responsible for CO/CO_2 relative ration in the mixture. Since RWGS is always shifted towards the reactants, refit procedure has reasonably identified the CO_2-to-methanol as the preferential chemical path to synthesize methanol.

Finally, the comparison among refit and VBF model bring out some discrepancies: reactions are close to equilibrium (i.e. negligible rates) close to the tube exit, while, according to proposed model, there is still space to produce methanol.

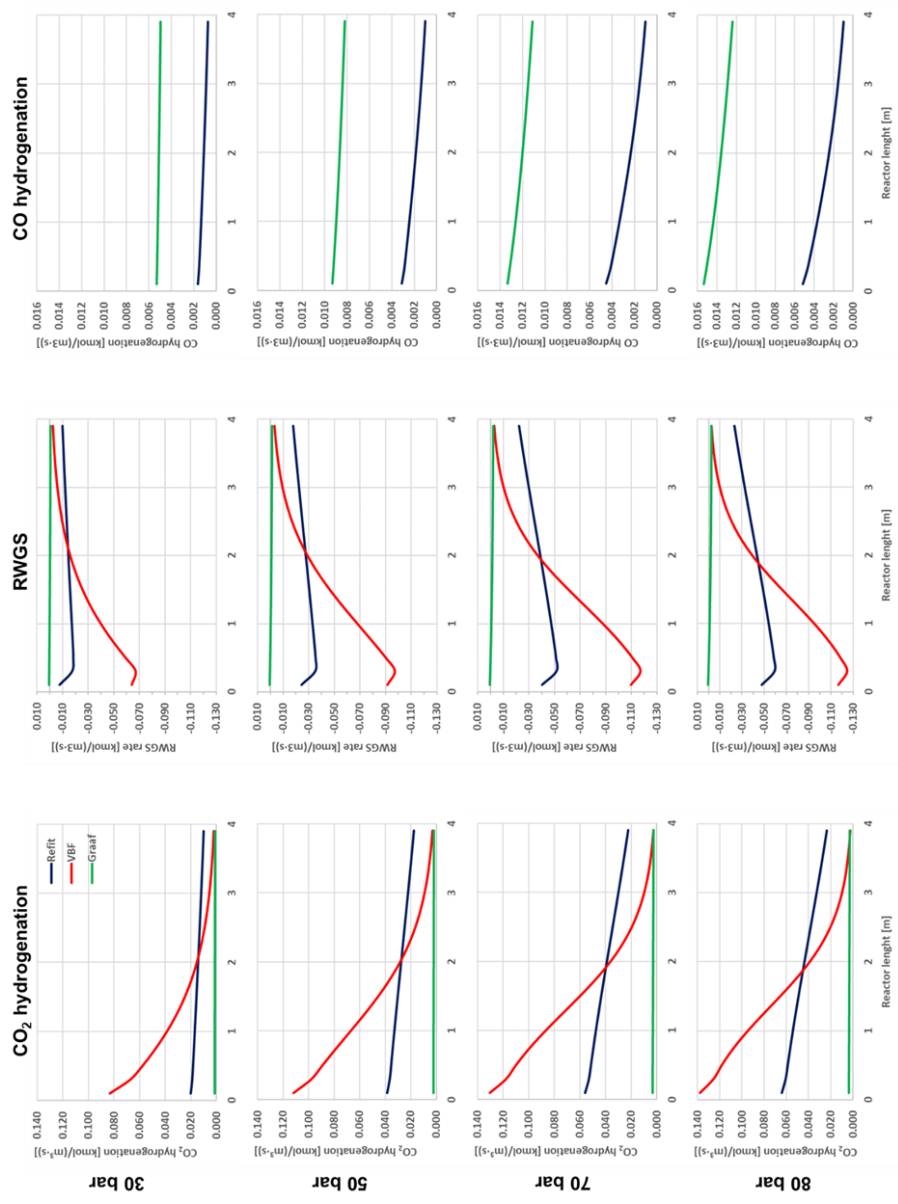

Figure 23 - reaction rates in the methanol synthesis reactor at different pressures with bio-syngas feed composition as reported in Table 10~~Table 10~~

CONCLUSIONS

In one century of bulk production, methanol became one of the most relevant molecules for our society. Many trends have been discussed in terms of process technologies, catalyst development, and ideal feedstocks, emphasizing the recent excitement around this compound. Nevertheless, few enhancements only have been proposed in kinetic models and kinetic parameters. Despite there is still a lack of understanding in the relevance of kinetic paths (from CO and/or CO_2) in methanol synthesis, the existing models proposed by Graaf et al. and Vanden Bussche and Froment reasonably suit for the purpose of predicting reactant conversion and methanol production. In any case, the present work is aimed at updating, or better still refitting, the original Graaf model to improve the accuracy of the methanol synthesis on CZA catalyst even in presence of slight differences in the catalyst preparation and/or formulation.

This work reflects the effect that the change in process operating conditions of the methanol synthesis process has on the prediction accuracy of the most popular kinetic models. It was shown how by means of refitting the kinetic parameters of the classical models on datasets more representative of current operating conditions better predictions could be achieved. The most used Graaf and VBF models are demonstrated to be reasonably good to describe methanol synthesis rate. Nevertheless, they suffer from unreliable predictions in some operating ranges characterized by middle-low pressure and peculiar feed compositions which are not unrealistic in the next future [125,126]. The parameters refit enables to mitigate shortcomings related to the current industrial kinetics: from one side, the original Graaf model underestimates the methanol production, instead, VBF model overestimate the methanol amount in the product mixture. The proposed refitted model is more in general a trade-off of the two even though it has been shown that it exhibits more features loaned from the VBF kinetics.

It was proven that the Graaf prediction error could be greatly improved upon by means of robust refitting of its parameters and the validity range can be extended. Nonlinear regression coupled with outlier detection algorithm applied on a large-varied dataset is a suitable method for numerical refit of kinetic parameters to account for recent trends in industrial methanol synthesis and possible future developments such as recent interest in CO_2 as a feedstock. Furthermore, the analysis have been proven that the refitted model does not suffer any abnormal predictions or incoherent predictions, hence, the refitting procedure has been successfully accomplished. Finally, authors

would remark that the data analytics is not a common practice in chemical engineering and it has not been adopted in the most recent attempts of kinetics refit. Hence, the proposed procedure, which has been applied on the original Graaf model, is a powerful and general framework that could be applied also to any kind of kinetic model which needs coefficients updating.

Acknowledgments

Authors gratefully acknowledge the invaluable support of Ing. Martina Cauteruccio and Ing. Veronica Gallo for their works during the M.Sc. Thesis Project.

SYNOPSIS (GRAPHIL ABSTRACT)

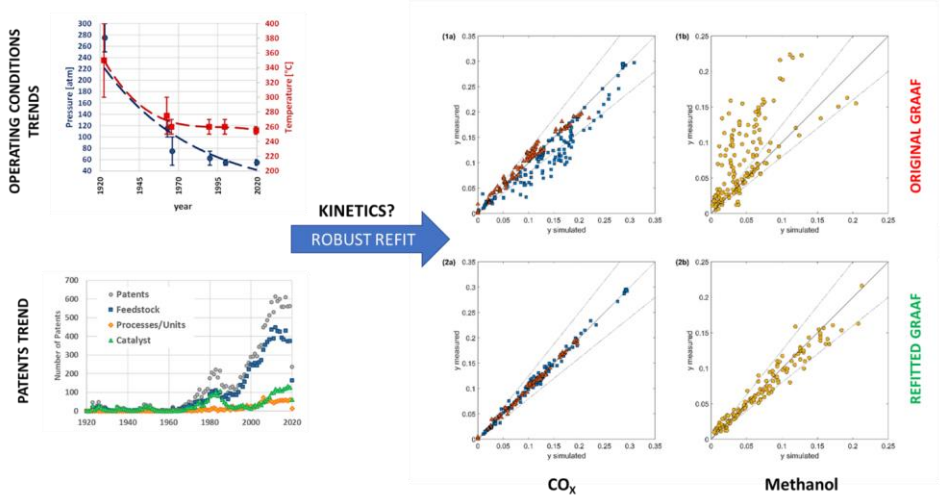

ASSOCIATED CONTENT

APPENDIX A

Table A1 - General form of kinetic rates in Graaf model

Reactions	Reaction rates
$CO_2 + 3H_2 \rightarrow CH_3OH + H_2O$	$r_{CO_2/MeOH} = \frac{k_1 K_{CO_2}\left(f_{CO_2} f_{H_2}^{\frac{3}{2}} - \frac{f_{MeOH} f_{H_2O}}{f_{H_2}^{\frac{3}{2}} K_{eqCO_2}}\right)}{DEN}$
$CO_2 + H_2 \rightarrow CO + H_2O$	$r_{RWGS} = \frac{k_2 K_{CO_2}\left(f_{CO_2} f_{H_2} - \frac{f_{H_2O} f_{CO}}{K_{eqRWGS}}\right)}{DEN}$
$CO + 2H_2 \rightarrow CH_3OH$	$r_{CO/MeOH} = \frac{k_3 K_{CO}\left(f_{CO} f_{H_2}^{\frac{3}{2}} - \frac{f_{MeOH}}{f_{H_2}^{\frac{1}{2}} K_{eqCO}}\right)}{DEN}$
$DEN = (1 + K_{CO} f_{CO} + K_{CO_2} f_{CO_2})(f_{H_2}{}^{1/2} + (K_{H_2O}/K_{H_2}{}^{1/2}) f_{H_2O})$	

Table A2 - Comparison of refitted kinetic constants and adsorption constants in Graaf model

Parameters	Graaf [98]	Proposed Model
k_1	$1.09 \cdot 10^5 \, e^{-\frac{87500}{RT}}$	$9.205 \cdot 10^1 \, e^{-\frac{45889}{RT}}$
k_2	$9.64 \cdot 10^{11} \, e^{-\frac{152900}{RT}}$	$4.241 \cdot 10^{13} \, e^{-\frac{149856}{RT}}$
k_3	$4.89 \cdot 10^7 \, e^{-\frac{113000}{RT}}$	$2.240 \cdot 10^7 \, e^{-\frac{106729}{RT}}$
K_{CO_2}	$7.05 \cdot 10^{-7} \, e^{\frac{61700}{RT}}$	$1.540 \cdot 10^{-3} \, e^{\frac{14936}{RT}}$
K_{CO}	$2.16 \cdot 10^{-5} \, e^{\frac{46800}{RT}}$	$8.206 \cdot 10^{-9} \, e^{\frac{76594}{RT}}$
$K_{H_2O/K_{H_2}^{1/2}}$	$6.37 \cdot 10^{-9} \, e^{\frac{84000}{RT}}$	$3.818 \cdot 10^{-9} \, e^{\frac{97350}{RT}}$

APPENDIX B

The experimental data are grouped according to the source. The case identification number is the same provided in the results section of the article. The relative error is calculated as:

$$\epsilon_{\text{rel}}^{\text{Model}} = 1 - \frac{\text{X}_{\text{model}}}{\text{X}_{\text{exp-data}}}$$

Stoichiometric Number (SN) and Carbon Oxides Ratio (COR) definitions are reported:

$$\text{SN} = \frac{\text{y}_{\text{H2}} - \text{y}_{\text{CO}_2}}{\text{y}_{\text{CO}} + \text{y}_{\text{CO}_2}} \quad (4)$$

$$\text{COR} = \frac{\text{y}_{\text{CO}_2}}{\text{y}_{\text{CO}} + \text{y}_{\text{CO}_2}} \quad (5)$$

	Case	T [°C]	P [bar]	Flow in [mol/s]	COR	SN	$\varepsilon_{rel}^{Refit}$ [%]	$\varepsilon_{rel}^{Graaf}$ [%]	ε_{rel}^{VBF} [%]
Park [80]	1	250	50	9.92E-05	0.37	1.97	-8.95	-67.90	26.47
	2	270	50	9.92E-05	0.37	1.97	12.17	-25.37	14.28
	3	300	50	9.92E-05	0.37	1.97	3.57	3.49	-4.29
	4	320	50	9.92E-05	0.37	1.97	-2.52	-2.52	-9.21
	5	340	50	9.92E-05	0.37	1.97	-12.66	-12.66	-17.53
	6	250	50	3.97E-05	0.37	1.97	3.85	-48.08	2.40
	7	250	50	9.92E-05	0.37	1.97	-7.23	-67.29	28.86
	8	250	50	0.000149	0.37	1.97	-16.26	-72.50	37.62
	9	250	50	0.000198	0.37	1.97	-22.57	-75.40	39.42
	10	250	50	3.97E-05	0.37	1.97	6.13	-46.94	4.65
	11	250	70	3.97E-05	0.37	1.97	8.08	-40.96	3.22
	12	250	90	3.97E-05	0.37	1.97	10.02	-34.04	3.10
	13	250	50	3.97E-05	1.00	2.00	7.21	1.60	-20.77
	14	250	50	3.97E-05	0.59	1.96	3.16	-36.68	1.34
	15	250	50	3.97E-05	0.39	2.00	5.24	-44.79	3.03
	16	250	50	3.97E-05	0.24	2.03	12.36	-45.42	10.49
	17	250	50	3.97E-05	0.16	1.94	13.37	-46.81	14.18
	18	250	50	3.97E-05	0.10	2.03	6.16	-46.73	13.01
	19	250	50	3.97E-05	0.07	2.07	1.93	-44.57	16.24
	20	250	50	3.97E-05	0.06	2.00	15.47	-37.69	33.06
	21	250	50	3.97E-05	0.00	1.97	-1.70	9.36	-100.00
	22	250	50	3.97E-05	0.36	2.04	-2.89	-49.95	-5.00
	23	250	50	3.97E-05	0.36	2.44	3.44	-43.06	0.75
	24	250	50	3.97E-05	0.35	3.50	9.06	-31.49	5.33
	25	250	50	3.97E-05	0.36	5.57	5.86	-19.15	0.88
	26	250	50	3.97E-05	0.37	1.97	2.54	-48.73	1.11
	27	250	50	3.97E-05	0.36	1.91	5.40	-38.25	-0.04
	28	250	70	3.97E-05	0.36	1.91	1.72	-37.27	-5.09
	29	250	70	3.97E-05	0.37	1.97	-1.18	-46.02	-5.63
	30	250	70	3.97E-05	1.00	2.00	-2.57	-10.22	-40.33
	31	250	70	3.97E-05	0.39	2.00	9.24	-37.76	4.10
	32	250	70	3.97E-05	0.24	2.03	18.10	-38.52	9.64
	33	250	70	3.97E-05	0.10	2.03	14.54	-40.60	9.78
	34	250	70	3.97E-05	0.06	2.00	15.58	-38.59	15.04
	35	250	70	3.97E-05	0.00	1.97	1.71	-0.59	-100.00
	36	270	70	3.97E-05	1.00	2.00	5.97	5.98	-13.87
	37	270	70	3.97E-05	0.39	2.00	16.03	10.47	6.34
	38	270	70	3.97E-05	0.24	2.03	18.35	11.77	8.44
	39	270	70	3.97E-05	0.10	2.03	22.30	15.38	12.25
	40	270	70	3.97E-05	0.06	2.00	19.35	12.85	10.15
	41	270	70	3.97E-05	0.00	1.97	19.24	22.62	-100.00
	42	250	50	3.97E-05	1.00	2.00	-7.44	-12.29	-31.60
	43	250	50	3.97E-05	1.00	2.41	3.93	-2.31	-24.01
	44	250	50	3.97E-05	1.00	3.71	1.69	-4.81	-25.75
	45	250	50	3.97E-05	1.00	6.17	-2.66	-8.01	-27.75
	46	250	60	3.97E-05	1.00	2.00	-1.76	-8.63	-34.10
	47	250	60	3.97E-05	1.00	2.41	3.26	-4.52	-31.69
	48	250	60	3.97E-05	1.00	3.71	4.30	-3.53	-31.34
	49	250	60	3.97E-05	1.00	6.17	-3.16	-8.89	-35.05
	50	250	70	3.97E-05	1.00	2.00	-1.45	-9.20	-39.65
	51	250	70	3.97E-05	1.00	2.41	3.56	-4.98	-37.62
	52	250	70	3.97E-05	1.00	3.71	9.94	1.21	-34.28
	53	250	70	3.97E-05	1.00	6.17	0.58	-5.30	-38.59
	54	250	80	3.97E-05	0.42	4.75	6.65	-6.56	-0.32
	55	260	80	3.97E-05	0.42	4.75	3.77	1.87	-3.43
	56	270	80	3.97E-05	0.42	4.75	-1.03	-1.10	-8.59
	57	270	80	4.96E-05	0.42	4.75	4.56	4.19	-3.42

	58	230	50	9.92E-05	0.37	1.97	-40.58	-85.62	6.77
	59	240	50	9.92E-05	0.37	1.97	-29.49	-80.37	16.59
	60	250	50	9.92E-05	0.37	1.97	-12.57	-69.18	21.44
	61	260	50	9.92E-05	0.37	1.97	2.87	-50.61	19.06
	62	270	50	9.92E-05	0.37	1.97	15.06	-23.44	17.24
	63	280	50	9.92E-05	0.37	1.97	12.74	-2.96	7.40
	64	290	50	9.92E-05	0.37	1.97	4.31	1.68	-3.17
	65	300	50	9.92E-05	0.37	1.97	6.90	6.81	-1.22
	66	310	50	9.92E-05	0.37	1.97	13.63	13.63	5.31
	67	320	50	9.92E-05	0.37	1.97	14.84	14.84	6.96
	68	340	50	9.92E-05	0.37	1.97	-26.41	-26.41	-30.51
	69	230	50	9.92E-05	0.35	4.53	-35.26	-81.31	-34.68
	70	240	50	9.92E-05	0.35	4.53	-22.40	-72.94	-18.64
	71	250	50	9.92E-05	0.35	4.53	-4.48	-56.11	-0.14
	72	260	50	9.92E-05	0.35	4.53	4.29	-34.22	5.52
	73	270	50	9.92E-05	0.35	4.53	8.46	-10.15	5.75
	74	280	50	9.92E-05	0.35	4.53	10.46	6.34	4.89
	75	290	50	9.92E-05	0.35	4.53	8.20	8.20	1.38
	76	300	50	9.92E-05	0.35	4.53	8.25	8.30	1.11
	77	230	50	3.97E-05	0.37	1.97	-20.30	-78.30	12.66
	78	240	50	3.97E-05	0.37	1.97	-1.31	-65.64	12.04
	79	250	50	3.97E-05	0.37	1.97	8.47	-45.77	6.95
	80	270	50	3.97E-05	0.37	1.97	10.19	0.72	1.96
	81	230	50	3.97E-05	0.35	4.53	-11.91	-68.67	-16.51
	82	240	50	3.97E-05	0.35	4.53	2.55	-50.01	-1.16
	83	250	50	3.97E-05	0.35	4.53	6.91	-25.56	2.44
	84	260	50	3.97E-05	0.35	4.53	4.98	-5.96	-0.50
	85	270	50	3.97E-05	0.35	4.53	7.10	5.50	0.75
	86	280	50	3.97E-05	0.35	4.53	0.44	0.39	-5.95
	87	290	50	3.97E-05	0.35	4.53	-8.19	-8.19	-14.23
	88	300	50	3.97E-05	0.35	4.53	-17.85	-17.85	-23.27
	89	250	70	9.92E-05	0.36	2.04	-2.53	-63.99	19.99
	90	220	70	9.92E-05	0.36	2.04	-41.16	-84.77	-11.51
	91	230	70	9.92E-05	0.36	2.04	-45.61	-85.69	-17.07
	92	240	70	9.92E-05	0.36	2.04	-26.01	-78.10	5.64
	93	250	70	9.92E-05	0.36	2.04	0.70	-62.79	23.97
	94	260	70	9.92E-05	0.36	2.04	16.17	-41.85	22.80
	95	270	70	9.92E-05	0.36	2.04	24.75	-13.69	20.15
	96	280	70	9.92E-05	0.36	2.04	31.97	16.47	22.08
	97	300	70	9.92E-05	0.36	2.04	20.89	20.81	10.09
	98	250	70	9.92E-05	0.36	2.04	0.50	-62.87	23.72
	99	300	70	9.92E-05	0.36	2.04	22.18	22.09	11.27
	100	250	70	9.92E-05	0.36	2.04	-1.41	-63.57	21.37
	101	250	50	9.92E-05	0.36	2.04	-8.22	-67.15	24.89
	102	250	70	9.92E-05	0.36	2.04	9.50	-59.54	34.80
	103	250	90	9.92E-05	0.36	2.04	21.41	-52.68	37.99
	104	250	50	9.92E-05	1.00	2.00	2.32	-19.18	-23.90
	105	250	50	9.92E-05	0.59	1.96	5.42	-52.04	31.81
	106	250	50	9.92E-05	0.39	2.00	9.19	-59.99	47.57
	107	250	50	9.92E-05	0.24	2.03	-9.79	-69.23	29.01
	108	250	50	9.92E-05	0.10	2.03	-10.01	-63.73	46.09
	109	250	50	9.92E-05	0.06	2.00	-23.26	-64.09	27.08
	110	250	50	9.92E-05	0.00	1.97	-36.06	-28.91	-100.00
	111	250	50	3.97E-05	0.36	2.04	3.51	-46.66	1.26
	112	250	50	3.97E-05	0.35	3.50	-0.87	-37.73	-4.25
	113	250	50	3.97E-05	0.36	5.57	-3.11	-26.01	-7.67
	114	250	50	9.92E-05	0.36	2.04	19.74	-57.14	62.94
	115	250	50	9.92E-05	0.36	2.44	23.80	-53.29	59.68
	116	250	50	9.92E-05	0.35	3.50	21.62	-48.99	39.61

	117	250	50	9.92E-05	0.35	4.35	22.87	-43.95	31.15
	118	250	50	9.92E-05	0.36	5.57	26.60	-36.00	25.48

1

	Case	T [°C]	P [bar]	Flow in [mol/s]	COR	SN	$\varepsilon_{rel}^{Refit}$ [%]	$\varepsilon_{rel}^{Graaf}$ [%]	ε_{rel}^{VBF} [%]
in-house exp data, Previtali [49]	119	240.15	20	3.84E-05	0.20	2.41	-89.55	-37.84	8.13
	120	260.15	20	3.84E-05	0.20	2.41	-3.67	-5.96	-8.99
	121	240.15	20	3.85E-05	1.00	2.49	3.05	26.15	-3.25
	122	260.15	20	3.85E-05	1.00	2.49	-18.85	-16.15	-24.15
	123	240.15	20	3.84E-05	0.00	2.00	65.93	181.50	-100.00
	124	260.15	20	3.84E-05	0.00	2.00	-12.64	9.86	-100.00
	125	240.15	20	3.84E-05	0.00	2.01	75.60	195.28	-100.00
	126	260.15	20	3.47E-05	1.00	2.01	-51.90	-50.97	-55.18
	127	260.15	20	3.85E-05	0.00	2.00	12.98	38.07	-100.00
	128	240.15	20	3.85E-05	0.20	2.39	42.62	-17.45	39.83
	129	260.15	20	3.85E-05	0.20	2.39	13.63	11.32	7.33
	130	240.15	20	3.85E-05	1.00	2.49	-21.88	-4.40	-26.66
	131	260.15	20	3.85E-05	1.00	2.49	-44.64	-42.88	-48.26
	132	240.15	20	3.85E-05	0.00	2.00	29.09	117.27	-100.00
	133	260.15	20	3.85E-05	0.00	2.00	-1.62	21.08	-100.00

2

	Case	T [°C]	P [bar]	Flow in [mol/s]	COR	SN	$\varepsilon_{rel}^{Refit}$ [%]	$\varepsilon_{rel}^{Graaf}$ [%]	ε_{rel}^{VBF} [%]
Graaf [95]	134	210.5	20	0.000167	0.15	5.34	15.94	-80.35	38.33
	135	210.5	20	0.000223	0.15	5.34	17.31	-80.63	43.11
	136	210.5	20	0.000339	0.15	5.34	20.47	-80.75	52.26
	137	226.3	20	0.000177	0.15	5.34	-3.37	-72.43	41.07
	138	226.3	20	0.000235	0.15	5.34	-1.31	-72.79	52.83
	139	226.3	20	0.000256	0.15	5.34	-3.79	-73.70	51.38
	140	226.3	20	0.000318	0.15	5.34	-0.40	-73.29	62.80
	141	226.3	20	0.000355	0.15	5.34	-4.26	-74.54	59.24
	142	226.3	20	0.000378	0.15	5.34	-5.74	-75.05	58.35
	143	243.7	20	0.000175	0.15	5.34	-21.16	-53.48	12.89
	144	243.7	20	0.000278	0.15	5.34	-32.02	-62.27	15.97
	145	243.7	20	0.000339	0.15	5.34	-32.89	-63.46	22.49
	146	259.4	20	0.000205	0.15	5.34	-25.35	-28.47	-3.84
	147	259.4	20	0.000324	0.15	5.34	-37.81	-40.88	-1.36
	148	259.4	20	0.000387	0.15	5.34	-42.89	-45.86	-1.93
	149	259.4	20	0.000558	0.15	5.34	-47.91	-50.91	4.10
	150	259.4	20	0.000559	0.15	5.34	-44.09	-47.31	11.78
	151	259.4	20	0.000867	0.15	5.34	-48.95	-52.24	18.76
	152	259.4	20	0.001205	0.15	5.34	-51.95	-55.30	22.57
	153	274.8	20	0.000357	0.15	5.34	-28.09	-14.06	-7.92
	154	274.8	20	0.000576	0.15	5.34	-42.31	-25.05	-8.03
	155	274.8	20	0.000925	0.15	5.34	-50.98	-32.43	-3.86
	156	274.8	20	0.001108	0.15	5.34	-50.98	-31.31	3.14
	157	274.8	20	0.001430	0.15	5.34	-57.20	-38.94	-1.59
	158	274.8	20	0.001527	0.15	5.34	-55.02	-35.59	5.59
	159	274.8	20	0.001866	0.15	5.34	-56.18	-36.64	9.17

3

4

5

6

APPENDIX C

The main classification systems of patents are the International Patent Classification (IPC), adopted in more than 100 Patent Offices, and the Cooperative Patent Classification (CPC), managed by the European Patent Office (EPO) and United States Patent and Trademark Office (USPTO). They consist of eight and nine sections, respectively, which are further subdivided into classes, subclasses, groups, and subgroups defined by the different Patent Institution. The list of relevant PC/CPC subgroups is reported in Table C 1~~Table C 1~~.

Each of the listed subgroups has been properly combined as specified in Table C 2~~Table C 2~~, to retrieve the corresponding and relevant patent documents. The search strategy is reported in Table C 3~~Table C 3~~.

-

Table C 1 - List of main IPC/CPC subgroups for the industrial methanol synthesis

Subgroup	Definition
C07C 31/04 (IPC/CPC)	**Methanol**
C07C 29/15 (IPC/CPC)	Preparation of alcohols - by reduction of oxides of carbon exclusively
C07C 29/151 (IPC/CPC)	Preparation of alcohols - by reduction of oxides of carbon exclusively - **with hydrogen or hydrogen-containing gases**
C07C 29/1512 (CPC)	Preparation of alcohols by reduction of oxides of carbon exclusively - with hydrogen or hydrogen-containing gases – **characterized by reaction conditions**
C07C 29/1514 (CPC)	Preparation of alcohols by reduction of oxides of carbon exclusively - with hydrogen or hydrogen-containing gases – characterized by reaction conditions – **the solvents being characteristic**
C07C 29/1516 (CPC)	Preparation of alcohols by reduction of oxides of carbon exclusively - with hydrogen or hydrogen-containing gases – **Multi steps**
C07C 29/1518 (CPC)	Preparation of alcohols by reduction of oxides of carbon exclusively with hydrogen or hydrogen-containing gases – Multi steps – **one step being the formation of initial mixture of carbon oxides and hydrogen for synthesis**
C07C 29/152 (IPC/CPC)	Preparation of alcohols by reduction of oxides of carbon exclusively with hydrogen or hydrogen-containing gases – **characterized by the reactor used**
C07C 29/153 (IPC/CPC)	Preparation of alcohols by reduction of oxides of carbon exclusively with hydrogen or hydrogen-containing gases – **characterized by the catalysts used**
C07C 29/154 (IPC/CPC)	Preparation of alcohols by reduction of oxides of carbon exclusively with hydrogen or hydrogen-containing gases – characterized by the catalysts used – **containing copper, silver, gold, or compounds thereof**

C07C 29/156 (IPC/CPC)	Preparation of alcohols by reduction of oxides of carbon exclusively with hydrogen or hydrogen-containing gases – characterized by the catalysts used – **containing iron group metals, platinum group metals, or compounds thereof**
C07C 29/157 (IPC/CPC)	Preparation of alcohols by reduction of oxides of carbon exclusively with hydrogen or hydrogen-containing gases – characterized by the catalysts used – containing iron group metals, platinum group metals or compounds thereof - **containing platinum group metals or compounds thereof**
C07C 29/158 (IPC/CPC)	Preparation of alcohols by reduction of oxides of carbon exclusively with hydrogen or hydrogen-containing gases – characterized by the catalysts used – containing iron group metals, platinum group metals or compounds thereof - containing platinum group metals or compounds thereof - **containing rhodium or compounds thereof**
C07C 29/159 (IPC/CPC)	Preparation of alcohols by reduction of oxides of carbon exclusively with hydrogen or hydrogen-containing gases – **with reducing agents other than hydrogen or hydrogen-containing gases**
C07F 1/08 (IPC/CPC)	Copper compunds
C07F 3/06 (IPC/CPC)	Zinc compounds
C07F 5/06(IPC/CPC)	Aluminium compounds
C01F 7/02 (IPC/CPC)	Aluminum oxide, aluminum hydroxide, aluminates
B01J 21/04 (IPC/CPC)	Catalysts comprising the elements, oxides, or hydroxides of magnesium, boron, aluminum, carbon, silicon, titanium, zirconium, or hafnium - Boron or aluminum; Oxides or hydroxides thereof – **Alumina**
B01J 23/72 (IPC/CPC)	Catalysts comprising metals or metal oxides or hydroxides – of the iron group metals or copper – **copper**
B01J 23/80 (IPC/CPC)	Catalysts comprising metals or metal oxides or hydroxides – of the iron group metals or copper – combined with metals, oxides or hydroxides – with **zinc**, cadmium or mercury
C01B 32/50 (IPC/CPC)	Carbon dioxide
C07B 61/00 (IPC/CPC)	Other general methods
B01J 31/1691 (CPC)	Metal-organic frameworks (MOF)

Table C 2 - Combination of classification symbols

Objective	**Combination of classification symbols**

Preparation of methanol starting from syngas	{[C07C 31/04 AND (C07C 29/15 OR C07C 29/151 OR C07C 29/1512 OR C07C 29/1514 OR C07C 29/1516 OR C7C 29/1518 OR C07C 29/152 OR C07C 29/153 OR C07C 29/154 OR C07C 29/1518]}
Preparation of methanol with CO_2	{[C07C 31/04 AND (C07C 29/151 OR C07C 29/152 OR C07C 29/154 OR C07C 29/159) AND C07B61/00]}
CZA catalyst	{[C07F 1/08 AND C07F 3/06 AND (C07F 5/06 OR C01F 7/02)] OR [B01J 21/04 AND B01J 23/72 AND B01J 23/80]}

1

2

3 Table C 3 - Search query results

Query No.	Results	Search query
1	11782	(C07F-005/06 OR C01F-007/02)/IPC
2	624	(C07F-001/08 AND C07F-003/06)/IPC
3	62	1 AND 2
4	98	(B01J-021/04 AND B01J-023/72 AND B01J-023/80)/IPC
5	160	3 OR 4
6	183	(CU_ZN_AL_2_O_3)/TI/AB/CLMS/ICLM/DESC/ODES
7	161	(CU W ZN W AL W "2" W O W "3")/TI/AB/CLMS/ICLM/DESC/ODES
8	342	5 OR 6 OR 7
9	4605	(C07C-029/151 OR C07C-029/152 OR C07C-029/153 OR C07C-029/154 OR C07C-029/156 OR C07C-029/157)/IPC
10	3051	(C07C-029/151 OR C07C-029/1512 OR C07C-029/1514 OR C07C-029/1516 C07C-029/1518 OR C07C-029/152 OR C07C-029/153 OR C07C-029/154 OI 029/156 OR C07C-029/157)/CPC
11	4851	9 OR 10
12	5407	(C07C-031/04)/IPC/CPC
13	320790	(METHANOL OR "CH3OH" OR ("C" W "H" W "3" W "O" W "H"))/TI/AB/CLMS/ICLM
14	3766	11 NOT "CO2"
15	3766	14 NOT "CARBON DIOXIDE"
16	2522	(12 OR 13) AND 15
17	1085	11 NOT 15
18	1508	("CO2" OR "CARBON DIOXIDE" OR ("C" W "O" W "2"))/TI/AB/CLMS/ICLM AND (C07B-061/00)/IPC/CPC

19	2503	17 OR 18
20	5523	(C07C-029/15+)/IPC/CPC
21	849	(METHANOL AND (CZA OR (COPPER_ZINC_ALUMINA) OR ("CU" W "ZN" W "AL" W "2" W "O" W "3")))/TI/AB/CLMS/ICLM/DESC/ODES
22	1068	8 OR 21
23	1147	(B01J-031/1691)/CPC
24	136	20 AND (COAL GASIFICATION)
25	262	20 AND (BIOMASS?)
26	276	20 AND (STEAM REFORMING)
27	257	20 AND (PARTIAL OXIDATION)
28	10	20 AND (SHALE OIL)
29	88	20 AND (AUTOTHERMAL)
30	893	(C07C-029/154)/IPC/CPC
31	868	30 NOT SILVER
32	854	31 NOT GOLD
33	1865	32 OR 22
34	893	33 AND 20
35	824	(C07C-029/156)/IPC/CPC
36	359	(C07C-029/157)/IPC/CPC
37	384	(C07C-029/158)/IPC/CPC
38	789	35 NOT PLATINUM
39	30009	("MOF" OR METAL_ORGANIC_FRAMEWORK)/TI/AB/CLMS/DESC/ODES/ICLM
40	39	20 AND (23 OR 39)

Formattato: Inglese (Regno Unito)

AUTHOR INFORMATION

Corresponding Author

* Flavio Manenti, flavio.manenti@polimi.it

Author Contributions

Funding Sources - This research has no external financial fund.

Notes

REFERENCES

(1) Sheldon, D. Methanol Production - A Technical History. *Johnson Matthey Technol. Rev.* **2017**, *61* (3), 172–182. https://doi.org/10.1595/205651317X695622.

(2) Olah, G. A. The Role of Catalysis in Replacing Oil by Renewable Methanol Using Carbon Dioxide Capture and Recycling (CCR). *Catal. Letters* **2013**, *143* (10), 983–987. https://doi.org/10.1007/s10562-013-1096-1.

(3) Olah, G. A.; Goeppert, A.; Prakash, G. K. S. Chemical Recycling of Carbon Dioxide to Methanol and Dimethyl Ether: From Greenhouse Gas to Renewable, Environmentally Carbon Neutral Fuels and Synthetic Hydrocarbons. *J. Org. Chem.* **2009**, *74* (2), 487–498. https://doi.org/10.1021/jo801260f.

(4) Goeppert, A.; Czaun, M.; Jones, J. P.; Surya Prakash, G. K.; Olah, G. A. Recycling of Carbon Dioxide to Methanol and Derived Products-Closing the Loop. *Chem. Soc. Rev.* **2014**, *43* (23), 7995–8048. https://doi.org/10.1039/c4cs00122b.

(5) Li, J.; Ma, X.; Liu, H.; Zhang, X. Life Cycle Assessment and Economic Analysis of Methanol Production from Coke Oven Gas Compared with Coal and Natural Gas Routes. *J. Clean. Prod.* **2018**, *185*, 299–308. https://doi.org/10.1016/j.jclepro.2018.02.100.

(6) Stephan, D. W. Catalysis: A Step Closer to a Methanol Economy. *Nature* **2013**, *495* (7439), 54–55. https://doi.org/10.1038/nature11955.

(7) Goeppert, A.; Olah, G. A.; Surya Prakash, G. K. *Toward a Sustainable Carbon Cycle: The Methanol Economy*; Elsevier Inc., 2018. https://doi.org/10.1016/B978-0-12-809270-5.00031-5.

(8) Olah, G. A. After Oil and Gas: Methanol Economy. *Catal. Letters* **2004**, *93* (1–2), 1–2. https://doi.org/10.1023/b:catl.0000017043.93210.9c.

(9) Roh, K.; Frauzem, R.; Gani, R.; Lee, J. H. Process Systems Engineering Issues and Applications towards Reducing Carbon Dioxide Emissions through Conversion Technologies. *Chem. Eng. Res. Des.* **2016**, *116*, 27–47. https://doi.org/10.1016/j.cherd.2016.10.007.

(10) Prasertsri, W.; Frauzem, R.; Suriyapraphadilok, U.; Gani, R. *Sustainable DME Synthesis-Design with CO2 Utilization*; Elsevier Masson SAS, 2016; Vol. 38. https://doi.org/10.1016/B978-0-444-63428-3.50185-5.

(11) Matzen, M.; Demirel, Y. Methanol and Dimethyl Ether from Renewable Hydrogen and Carbon Dioxide: Alternative Fuels Production and Life-Cycle Assessment. *J. Clean. Prod.* **2016**, *139*, 1068–1077. https://doi.org/10.1016/j.jclepro.2016.08.163.

(12) Haid, J.; Koss, U. Lurgi's Mega-Methanol Technology Opens the Door for a New Era in down-Stream Applications. *Stud. Surf. Sci. Catal.* **2001**, *136*, 399–404. https://doi.org/10.1016/s0167-2991(01)80336-0.

(13) Ogino, Y.; Oba, M.; Uchida, H. Catalytic Activity for Methanol Synthesis of Zinc Oxide-Chromium Oxide-Copper Oxide Catalysts and Its Structural Dependency. *Bull. Chem. Soc. Jpn.* **1960**, *33* (3), 358–363. https://doi.org/10.1246/bcsj.33.358.

(14) Mota, N.; Guil-Lopez, R.; Pawelec, B. G.; Fierro, J. L. G.; Navarro, R. M. Highly Active Cu/ZnO-Al Catalyst for Methanol Synthesis: Effect of Aging on Its Structure and Activity. *RSC Adv.* **2018**, *8* (37), 20619–20629. https://doi.org/10.1039/c8ra03291b.

(15) Etim, U. J.; Song, Y.; Zhong, Z. Improving the Cu/ZnO-Based Catalysts for Carbon Dioxide Hydrogenation to Methanol, and the Use of Methanol As a Renewable Energy Storage Media. *Front. Earth Sci.* **2020**, *8* (September), 1–26. https://doi.org/10.3389/fenrg.2020.545431.

(16) Aresta, M.; Karimi, I.; Kawi, S. *An Economy Based on Carbon Dioxide and Water Potential of Large Scale Carbon Dioxide Utilization: Potential of Large Scale Carbon Dioxide Utilization*; 2019. https://doi.org/10.1007/978-3-030-15868-2.

(17) Aresta, M. *Carbon Dioxide as Chemical Feedstock*; 2010. https://doi.org/10.1002/9783527629916.

(18) Tan, Z. *Air Pollution and Greenhouse Gases - From Basic Concepts to Engineering Applications for Air Emission Control*; Springer, 2014.

(19) Harald Heinrichs, Pim Martens Gerd Michelsen, A. W. *Sustainability Science - An Introduction*; Springer US, 2016. https://doi.org/10.1017/CBO9780511794469.

(20) Dibenedetto, A.; Tommasi, I. *Biological Utilization of Carbon Dioxide: The Marine Biomass Option*; 2003. https://doi.org/10.1007/978-94-017-0245-4_13.

(21) *Biorefinery: From Biomass to Chemicans and Fuels*; Aresta, M., Dibenedetto, A., Dumeignil, F., Eds.; De Gruyter, 2012.

(22) EU. Carbon capture, utilisation and storage.

(23) EU. Energy | Horizon 2020 https://ec.europa.eu/programmes/horizon2020/en/area/energy (accessed Dec 30, 2020).

(24) Yang, L.; Ge, X. Biogas and Syngas Upgrading. **2016**, *1*, 125–188. https://doi.org/10.1016/bs.aibe.2016.09.003.

(25) Blumberg, T.; Tsatsaronis, G.; Morosuk, T. On the Economics of Methanol Production from Natural Gas. *Fuel* **2019**, *256* (July), 115824. https://doi.org/10.1016/j.fuel.2019.115824.

(26) Abatzoglou, N.; Fauteux-Lefebvre, C. Review of Catalytic Syngas Production through Steam or Dry Reforming and Partial Oxidation of Studied Liquid Compounds. *Wiley Interdiscip. Rev. Energy Environ.* **2016**, *5* (2), 169–187. https://doi.org/10.1002/wene.167.

(27) Shahhosseini, H. R.; Iranshahi, D.; Saeidi, S.; Pourazadi, E.; Klemeš, J. J. Multi-Objective Optimisation of Steam Methane Reforming Considering Stoichiometric Ratio Indicator for Methanol Production. *J. Clean. Prod.* **2018**, *180*, 655–665. https://doi.org/10.1016/j.jclepro.2017.12.201.

(28) Quirino, P. P. S.; Amaral, A.; Pontes, K. V.; Rossi, F.; Manenti, F. Modeling and Simulation of an Industrial Top-Fired Methane Steam Reforming Unit. *Ind. Eng. Chem. Res.* **2020**, *59* (24), 11250–11264. https://doi.org/10.1021/acs.iecr.0c00456.

(29) Olsvik, O.; Hansen, R. High Pressure Autothermal Reforming (HP ATR). *Stud. Surf. Sci. Catal.* **1998**, *119*, 875–882. https://doi.org/10.1016/s0167-2991(98)80542-9.

(30) Jaggai, C.; Imkaraaz, Z.; Samm, K.; Pounder, A.; Koylass, N.; Chakrabarti, D. P.; Guo, M.; Ward, K. Towards Greater Sustainable Development within Current Mega-Methanol (MM) Production. *Green Chem.* **2020**, *22* (13), 4279–4294. https://doi.org/10.1039/d0gc01185a.

(31) Mirvakili, A.; Chahibakhsh, S.; Ebrahimzadehsarvestani, M.; Soroush, E.; Rahimpour, M.

R. Modeling and Assessment of Novel Configurations to Enhance Methanol Production in Industrial Mega-Methanol Synthesis Plant. *J. Taiwan Inst. Chem. Eng.* **2019**, *104*, 40–53. https://doi.org/10.1016/j.jtice.2019.09.018.

(32) Lange, J. P. Methanol Synthesis: A Short Review of Technology Improvements. *Catal. Today* **2001**, *64* (1–2), 3–8. https://doi.org/10.1016/S0920-5861(00)00503-4.

(33) De Klerk, A. *Transport Fuel. Biomass-, Coal-, Gas- and Waste-to-Liquids Processes.*; Elsevier Ltd, 2013. https://doi.org/10.1016/B978-0-08-099424-6.00012-0.

(34) Riaz, A.; Zahedi, G.; Klemeš, J. J. A Review of Cleaner Production Methods for the Manufacture of Methanol. *J. Clean. Prod.* **2013**, *57*, 19–37. https://doi.org/10.1016/j.jclepro.2013.06.017.

(35) Yang, C. J.; Jackson, R. B. China's Growing Methanol Economy and Its Implications for Energy and the Environment. *Energy Policy* **2012**, *41*, 878–884. https://doi.org/10.1016/j.enpol.2011.11.037.

(36) Chen, Z.; Shen, Q.; Sun, N.; Wei, W. Life Cycle Assessment of Typical Methanol Production Routes: The Environmental Impacts Analysis and Power Optimization. *J. Clean. Prod.* **2019**, *220* (2019), 408–416. https://doi.org/10.1016/j.jclepro.2019.02.101.

(37) Lan, W.; Chen, G.; Wang, C.; Zhu, X. Syngas Production from Biomass: A Review. *Adv. Mater. Res.* **2013**, *608–609*, 402–405. https://doi.org/10.4028/www.scientific.net/AMR.608-609.402.

(38) Göransson, K.; Söderlind, U.; He, J.; Zhang, W. Review of Syngas Production via Biomass

DFBGs. *Renew. Sustain. Energy Rev.* **2011**, *15* (1), 482–492. https://doi.org/10.1016/j.rser.2010.09.032.

(39) Guerrero, F.; Espinoza, L.; Ripoll, N.; Lisbona, P.; Arauzo, I.; Toledo, M. Syngas Production From the Reforming of Typical Biogas Compositions in an Inert Porous Media Reactor. *Front. Chem.* **2020**, *8* (March), 1–12. https://doi.org/10.3389/fchem.2020.00145.

(40) Bustan, M. D.; Haryati, S.; Hadiah, F.; Selpiana, S.; Huda, A. Syngas Production Improvement of Sugarcane Bagasse Conversion Using an Electromagnetic Modified Vacuum Pyrolysis Reactor. *Processes* **2020**, *8* (2), 1–9. https://doi.org/10.3390/pr8020252.

(41) Bassani, A.; Bozzano, G.; Pirola, C.; Frau, C.; Pettinau, A.; Maggio, E.; Ranzi, E.; Manenti, F. Sulfur Rich Coal Gasification and Low Impact Methanol Production. *J. Sustain. Dev. Energy, Water Environ. Syst.* **2018**, *6* (1), 210–226. https://doi.org/10.13044/j.sdewes.d5.0188.

(42) Bassani, A.; Pirola, C.; Maggio, E.; Pettinau, A.; Frau, C.; Bozzano, G.; Pierucci, S.; Ranzi, E.; Manenti, F. Acid Gas to Syngas (AG2S^{TM}) Technology Applied to Solid Fuel Gasification: Cutting H2S and CO2 Emissions by Improving Syngas Production. *Appl. Energy* **2016**, *184*, 1284–1291. https://doi.org/https://doi.org/10.1016/j.apenergy.2016.06.040.

(43) Bassani, A.; van Dijk, H. A. J.; Cobden, P. D.; Spigno, G.; Manzolini, G.; Manenti, F. Sorption Enhanced Water Gas Shift for H2 Production Using Sour Gases as Feedstock. *Int. J. Hydrogen Energy* **2019**, *44* (31), 16132–16143. https://doi.org/10.1016/j.ijhydene.2019.04.199.

(44) Bozzano, G.; Manenti, F. Efficient Methanol Synthesis: Perspectives, Technologies and Optimization Strategies. *Prog. Energy Combust. Sci.* **2016**, *56*, 71–105. https://doi.org/https://doi.org/10.1016/j.pecs.2016.06.001.

(45) Levi, P.; Vass, T.; Mandovà, H.; Gouy, A.; Schröder, A. Chemicals - IEA Tracking report https://www.iea.org/reports/chemicals.

(46) IEA. The challenge of reaching zero emissions in heavy industry www.iea.org/articles/the-challenge-of-reaching-zero-emissions-in-heavy-industry.

(47) IEA. Energy Technology Perspectives 2020. https://doi.org/10.1787/ab43a9a5-en.

(48) Nestler, F.; Schütze, A. R.; Ouda, M.; Hadrich, M. J.; Schaadt, A.; Bajohr, S.; Kolb, T. Kinetic Modelling of Methanol Synthesis over Commercial Catalysts: A Critical Assessment. *Chem. Eng. J.* **2020**, *394*, 124881. https://doi.org/https://doi.org/10.1016/j.cej.2020.124881.

(49) Previtali, D.; Longhi, M.; Galli, F.; Di Michele, A.; Manenti, F.; Signoretto, M.; Menegazzo, F.; Pirola, C. Low Pressure Conversion of CO2 to Methanol over Cu/Zn/Al Catalysts. The Effect of Mg, Ca and Sr as Basic Promoters. *Fuel* **2020**, *274*, 117804. https://doi.org/https://doi.org/10.1016/j.fuel.2020.117804.

(50) Leonzio, G. Mathematical Modeling of a Methanol Reactor by Using Different Kinetic Models. *J. Ind. Eng. Chem.* **2020**, *85*, 130–140. https://doi.org/10.1016/j.jiec.2020.01.033.

(51) Wörsdörfer, M. (IEA). *The Future of Petrochemicals*; 2018. https://doi.org/10.1787/9789264307414-en.

(52) IEA. The Future of Petrochemicals. *Futur. petrochemicals* **2018**. https://doi.org/10.1787/9789264307414-en.

(53) Xu, D.; Ding, M.; Hong, X.; Liu, G. Mechanistic Aspects of the Role of K Promotion on Cu−Fe-Based Catalysts for Higher Alcohol Synthesis from CO2 Hydrogenation. *ACS Catal.* **2020**, *10* (24), 14516–14526. https://doi.org/10.1021/acscatal.0c03575.

(54) Xu, Y.; Ma, H.; Zhang, H.; Qian, W.; Sun, Q.; Ying, W.; Chen, D. Cu-Promoted Iron Catalysts Supported on Nanorod-Structured Mn-Ce Mixed Oxides for Higher Alcohol Synthesis from Syngas. *Catalysts* **2020**, *10* (10), 1–12. https://doi.org/10.3390/catal10101124.

(55) Dang, S.; Yang, H.; Gao, P.; Wang, H.; Li, X.; Wei, W.; Sun, Y. A Review of Research Progress on Heterogeneous Catalysts for Methanol Synthesis from Carbon Dioxide Hydrogenation. *Catal. Today* **2019**, *330* (April 2018), 61–75. https://doi.org/10.1016/j.cattod.2018.04.021.

(56) Agarwal, R. A. *Methanol Synthesis from CO2 Hydrogenation Using Metal–Organic Frameworks*; Springer Singapore, 2019. https://doi.org/10.1007/978-981-13-3296-8_6.

(57) Stolar, T.; Prašnikar, A.; Martinez, V.; Karadeniz, B.; Bjelić, A.; Mali, G.; Friščić, T.; Likozar, B.; Užarević, K. Scalable Mechanochemical Amorphization of Bimetallic Cu-Zn MOF-74 Catalyst for Selective CO2reduction Reaction to Methanol. *ACS Appl. Mater. Interfaces* **2021**, *13* (2), 3070–3077. https://doi.org/10.1021/acsami.0c21265.

(58) Pustovarenko, A.; Dikhtiarenko, A.; Bavykina, A.; Gevers, L.; Ramírez, A.; Russkikh, A.; Telalovic, S.; Aguilar, A.; Hazemann, J. L.; Ould-Chikh, S.; Gascon, J. Metal-Organic

Framework-Derived Synthesis of Cobalt Indium Catalysts for the Hydrogenation of CO2 to Methanol. *ACS Catal.* **2020**, *10* (9), 5064–5076. https://doi.org/10.1021/acscatal.0c00449.

(59) Leduc, S.; Lundgren, J.; Franklin, O.; Dotzauer, E. Location of a Biomass Based Methanol Production Plant: A Dynamic Problem in Northern Sweden. *Appl. Energy* **2010**, *87* (1), 68–75. https://doi.org/10.1016/j.apenergy.2009.02.009.

(60) Peduzzi, E.; Tock, L.; Boissonnet, G.; Maréchal, F. Thermo-Economic Evaluation and Optimization of the Thermo-Chemical Conversion of Biomass into Methanol. *Energy* **2013**, *58*, 9–16. https://doi.org/10.1016/j.energy.2013.05.029.

(61) Specht, M.; Bandi, A.; Baumgart, F.; Murray, C. N.; Gretz, J. *Synthesis of Methanol from Biomass/CO2 Resources*; Elsevier Science Ltd: United Kingdom, 1999.

(62) Christensen, T. S.; Primdahl Copenhagen (Denmark)], I. I. [Haldor T. Improve Syngas Production Using Autothermal Reforming. **1994**.

(63) Yoon, H. C.; Erickson, P. A. Hydrogen from Coal-Derived Methanol via Autothermal Reforming Processes. *Int. J. Hydrogen Energy* **2008**, *33* (1), 57–63. https://doi.org/10.1016/j.ijhydene.2007.08.031.

(64) Franco, A.; Diaz, A. R. The Future Challenges for "Clean Coal Technologies": Joining Efficiency Increase and Pollutant Emission Control. *Energy* **2009**, *34* (3), 348–354. https://doi.org/10.1016/j.energy.2008.09.012.

(65) Chen, W.; Xu, R. Clean Coal Technology Development in China. *Energy Policy* **2010**, *38* (5), 2123–2130. https://doi.org/10.1016/j.enpol.2009.06.003.

(66) Chang, S.; Zhuo, J.; Meng, S.; Qin, S.; Yao, Q. Clean Coal Technologies in China: Current Status and Future Perspectives. *Engineering* **2016**, *2* (4), 447–459. https://doi.org/10.1016/J.ENG.2016.04.015.

(67) Xu, X.; Liu, Y.; Zhang, F.; Di, W.; Zhang, Y. Clean Coal Technologies in China Based on Methanol Platform. *Catal. Today* **2017**, *298* (May), 61–68. https://doi.org/10.1016/j.cattod.2017.05.070.

(68) Tang, X.; Snowden, S.; McLellan, B. C.; Höök, M. Clean Coal Use in China: Challenges and Policy Implications. *Energy Policy* **2015**, *87*, 517–523. https://doi.org/10.1016/j.enpol.2015.09.041.

(69) Fan, L. S.; Jadhav, R. A. Clean Coal Technologies: OSCAR and CARBONOX Commercial Demonstrations. *AIChE J.* **2002**, *48* (10), 2115–2123. https://doi.org/10.1002/aic.690481003.

(70) IEA. *The Future of Hydrogen - Seizing Today's Opportunity*; 2019. https://doi.org/10.1787/1e0514c4-en.

(71) Moulijn, J. A. *Chemical Process Technology*; 2013; Vol. 51. https://doi.org/10.5860/choice.51-2107.

(72) Klaus Weissermel, H. A. *Industrial Organic Chemistry*; Verlagsgesellschaft, V., Ed.; Wiley Online Books; John Wiley & Sons, 2003. https://doi.org/doi:10.1002/9783527619191.fmatter.

(73) Villa, P.; Forzatti, P.; Buzzi-Ferraris, G.; Garone, G.; Pasquon, I. Synthesis of Alcohols

from Carbon Oxides and Hydrogen. 1. Kinetics of the Low-Pressure Methanol Synthesis. *Ind. Eng. Chem. Process Des. Dev.* **1985**, *24* (1), 12–19. https://doi.org/10.1021/i200028a003.

(74) Klier, K.; Chatikavanij, V.; Herman, R. G.; Simmons, G. W. Catalytic Synthesis of Methanol from COH2: IV. The Effects of Carbon Dioxide. *J. Catal.* **1982**, *74* (2), 343–360. https://doi.org/https://doi.org/10.1016/0021-9517(82)90040-9.

(75) McNeil, M. A.; Schack, C. J.; Rinker, R. G. Methanol Synthesis from Hydrogen, Carbon Monoxide and Carbon Dioxide over a CuO/ZnO/Al2O3 Catalyst: II. Development of a Phenomenological Rate Expression. *Appl. Catal.* **1989**, *50* (1), 265–285. https://doi.org/https://doi.org/10.1016/S0166-9834(00)80841-6.

(76) Ma, H.; Ying, W.; Fang, D. Study on Methanol Synthesis from Coal-Based Syngas. *J. Coal Sci. Eng.* **2009**, *15* (1), 98–103. https://doi.org/10.1007/s12404-009-0120-y.

(77) Graaf, G. H.; Stamhuis, E. J.; Beenackers, A. A. C. M. Kinetics of Low-Pressure Methanol Synthesis. *Chem. Eng. Sci.* **1988**, *43* (12), 3185–3195. https://doi.org/https://doi.org/10.1016/0009-2509(88)85127-3.

(78) Takagawa, M.; Ohsugi, M. Study on Reaction Rates for Methanol Synthesis from Carbon Monoxide, Carbon Dioxide, and Hydrogen. *J. Catal.* **1987**, *107* (1), 161–172. https://doi.org/https://doi.org/10.1016/0021-9517(87)90281-8.

(79) Seidel, C.; Jörke, A.; Vollbrecht, B.; Seidel-Morgenstern, A.; Kienle, A. Kinetic Modeling of Methanol Synthesis from Renewable Resources. *Chem. Eng. Sci.* **2018**, *175*, 130–138. https://doi.org/https://doi.org/10.1016/j.ces.2017.09.043.

(80) Park, N.; Park, M.-J.; Lee, Y.-J.; Ha, K.-S.; Jun, K.-W. Kinetic Modeling of Methanol Synthesis over Commercial Catalysts Based on Three-Site Adsorption. *Fuel Process. Technol.* **2014**, *125*, 139–147. https://doi.org/10.1016/j.fuproc.2014.03.041.

(81) Lim, H.-W.; Park, M.-J.; Kang, S.-H.; Chae, H.-J.; Bae, J. W.; Jun, K.-W. Modeling of the Kinetics for Methanol Synthesis Using Cu/ZnO/Al2O3/ZrO2 Catalyst: Influence of Carbon Dioxide during Hydrogenation. *Ind. Eng. Chem. Res.* **2009**, *48* (23), 10448–10455. https://doi.org/10.1021/ie901081f.

(82) Vanden Bussche, K. M.; Froment, G. F. A Steady-State Kinetic Model for Methanol Synthesis and the Water Gas Shift Reaction on a Commercial Cu/ZnO/Al2O3Catalyst. *J. Catal.* **1996**, *161* (1), 1–10. https://doi.org/https://doi.org/10.1006/jcat.1996.0156.

(83) Kubota, T.; Hayakawa, I.; Mabuse, H.; Mori, K.; Ushikoshi, K.; Watanabe, T.; Saito, M. Kinetic Study of Methanol Synthesis from Carbon Dioxide and Hydrogen. *Appl. Organomet. Chem.* **2001**, *15* (2), 121–126. https://doi.org/10.1002/1099-0739(200102)15:2<121::AID-AOC106>3.0.CO;2-3.

(84) Askgaard, T. S.; Norskov, J. K.; Ovesen, C. V; Stoltze, P. A Kinetic Model of Methanol Synthesis. *J. Catal.* **1995**, *156* (2), 229–242. https://doi.org/https://doi.org/10.1006/jcat.1995.1250.

(85) Skrzypek, J.; Lachowska, M.; Moroz, H. Kinetics of Methanol Synthesis over Commercial Copper/Zinc Oxide/Alumina Catalysts. *Chem. Eng. Sci.* **1991**, *46* (11), 2809–2813. https://doi.org/https://doi.org/10.1016/0009-2509(91)85150-V.

(86) Løvik, I.; Rønnekleiv, M.; Olsvik, O.; Hertzberg, T. Estimation of a Deactivation Model for

the Methanol Synthesis Catalyst from Historic Process Data. In *European Symposium on Computer Aided Process Engineering - 11*; Gani, R., Jørgensen, S. B. B. T.-C. A. C. E., Eds.; Elsevier, 2001; Vol. 9, pp 219–224. https://doi.org/https://doi.org/10.1016/S1570-7946(01)80032-8.

(87) Nestler, F.; Krüger, M.; Full, J.; Hadrich, M. J.; White, R. J.; Schaadt, A. Methanol Synthesis – Industrial Challenges within a Changing Raw Material Landscape. *Chemie Ing. Tech.* **2018**, *90* (10), 1409–1418. https://doi.org/10.1002/cite.201800026.

(88) Ushikoshi, K.; Mori, K.; Kubota, T.; Watanabe, T.; Saito, M. Methanol Synthesis from CO2 and H2 in a Bench-Scale Test Plant. *Appl. Organomet. Chem. - APPL ORGANOMETAL CHEM* **2000**, *14*, 819–825. https://doi.org/10.1002/1099-0739(200012)14:123.0.CO;2-#.

(89) Bell, A. T. *Molecular Design of Highly Active Methanol Synthesis Catalysts*; Elsevier Masson SAS, 2001; Vol. 136. https://doi.org/10.1016/s0167-2991(01)80273-1.

(90) Spath, P. L.; Dayton, D. C. *Technical and Economic Assessment of Synthesis Gas to Fuels and Chemicals with Emphasis on the Potential for Biomass-Derived Syngas*; United States, 2003. https://doi.org/10.2172/15006100.

(91) Pavlišič, A.; Huš, M.; Prašnikar, A.; Likozar, B. Multiscale Modelling of CO2 Reduction to Methanol over Industrial Cu/ZnO/Al2O3 Heterogeneous Catalyst: Linking Ab Initio Surface Reaction Kinetics with Reactor Fluid Dynamics. *J. Clean. Prod.* **2020**, *275*. https://doi.org/10.1016/j.jclepro.2020.122958.

(92) Prašnikar, A.; Jurković, D. L.; Likozar, B. Reaction Path Analysis of CO2 Reduction to Methanol through Multisite Microkinetic Modelling over Cu/ZnO/Al2O3 Catalysts. *Appl.*

Catal. B Environ. **2021**, *292* (March), 2–11. https://doi.org/10.1016/j.apcatb.2021.120190.

(93) Manenti, F.; Buzzi-Ferraris, G. Criteria for Outliers Detection in Nonlinear Regression Problems. In *19 European Symposium on Computer Aided Process Engineering*; Jeżowski, J., Thullie, J. B. T.-C. A. C. E., Eds.; Elsevier, 2009; Vol. 26, pp 913–917. https://doi.org/https://doi.org/10.1016/S1570-7946(09)70152-X.

(94) Zhang, Q.; Martín, M.; Grossmann, I. E. Integrated Design and Operation of Renewables-Based Fuels and Power Production Networks. *Comput. Chem. Eng.* **2019**, *122*, 80–92. https://doi.org/10.1016/j.compchemeng.2018.06.018.

(95) Graaf, G. *The Synthesis of Methanol in Gas-Solid and Gas-Slurry Reactors - PhD Thesis, 1988*; 2016. https://doi.org/10.13140/RG.2.1.1002.8402.

(96) Buzzi-Ferraris, G.; Manenti, F. Interpolation and Regression Models for the Chemical Engineer. Solving Numerical Problems. **2010**.

(97) Buzzi-Ferraris, G.; Manenti, F. Data Interpretation and Correlation. *Kirk-Othmer Encyclopedia*; Wiley, New York, USA, 2011.

(98) Graaf, G. H.; Scholtens, H.; Stamhuis, E. J.; Beenackers, A. A. C. M. Intra-Particle Diffusion Limitations in Low-Pressure Methanol Synthesis. *Chem. Eng. Sci.* **1990**, *45* (4), 773–783. https://doi.org/https://doi.org/10.1016/0009-2509(90)85001-T.

(99) Graaf, G. H.; Sijtsema, P. J. J. M.; Stamhuis, E. J.; Joosten, G. E. H. Chemical Equilibria in Methanol Synthesis. *Chem. Eng. Sci.* **1986**, *41* (11), 2883–2890. https://doi.org/https://doi.org/10.1016/0009-2509(86)80019-7.

(100) Susanti, Y.; Pratiwi, H.; H., S.; Liana, T. M Estimation, S Estimation, and MM Estimation in Robust Regression. *Int. J. Pure Appl. Math.* **2014**, *91*. https://doi.org/10.12732/ijpam.v91i3.7.

(101) Chen, L.; Jiang, Q.; Song, Z.; Posarac, D. Optimization of Methanol Yield from a Lurgi Reactor. *Chem. Eng. Technol.* **2011**, *34* (5), 817–822. https://doi.org/10.1002/ceat.201000282.

(102) Bos, M. J.; Slotboom, Y.; Kersten, S. R. A.; Brilman, D. W. F. 110th Anniversary: Characterization of a Condensing CO2 to Methanol Reactor. *Ind. Eng. Chem. Res.* **2019**, *58* (31), 13987–13999. https://doi.org/10.1021/acs.iecr.9b02576.

(103) Slotboom, Y.; Bos, M. J.; Pieper, J.; Vrieswijk, V.; Likozar, B.; Kersten, S. R. A.; Brilman, D. W. F. Critical Assessment of Steady-State Kinetic Models for the Synthesis of Methanol over an Industrial Cu/ZnO/Al2O3 Catalyst. *Chem. Eng. J.* **2020**, *389* (December 2019), 124181. https://doi.org/10.1016/j.cej.2020.124181.

(104) Rousseeuw, P. J. Least Median of Squares Regression. *J. Am. Stat. Assoc.* **1984**, *79* (388), 871–880. https://doi.org/10.1080/01621459.1984.10477105.

(105) Buzzi-Ferraris, G.; Manenti, F. Outlier Detection in Large Data Sets. *Comput. Chem. Eng.* **2011**, *35* (2), 388–390. https://doi.org/10.1016/j.compchemeng.2010.11.004.

(106) Romagnoli, J. A.; Sánchez, M. C. *Data Processing and Reconciliation for Chemical Process Operations*; Romagnoli, J. A., Sánchez, M. C. B. T.-P. S. E., Eds.; Academic Press, 1999; Vol. 2. https://doi.org/https://doi.org/10.1016/S1874-5970(00)80020-X.

(107) Franceschini, G.; Macchietto, S. Model-Based Design of Experiments for Parameter Precision: State of the Art. *Chem. Eng. Sci.* **2008**, *63* (19), 4846–4872. https://doi.org/https://doi.org/10.1016/j.ces.2007.11.034.

(108) Tjoa, I. B.; Biegler, L. T. Simultaneous Strategies for Data Reconciliation and Gross Error Detection of Nonlinear Systems. *Comput. Chem. Eng.* **1991**, *15* (10), 679–690. https://doi.org/https://doi.org/10.1016/0098-1354(91)85014-L.

(109) Motulsky, H. J.; Brown, R. E. Detecting Outliers When Fitting Data with Nonlinear Regression – a New Method Based on Robust Nonlinear Regression and the False Discovery Rate. *BMC Bioinformatics* **2006**, *7* (1), 123. https://doi.org/10.1186/1471-2105-7-123.

(110) Hampel, F. R.; Ronchetti, E. M.; Rousseeuw, P. J.; Stahel, W. A. *Robust Statistics: The Approach Based on Influence Functions*; Wiley Series in Probability and Statistics; Wiley, 2011.

(111) Massart, D. L.; Kaufman, L.; Rousseeuw, P. J.; Leroy, A. Least Median of Squares: A Robust Method for Outlier and Model Error Detection in Regression and Calibration. *Anal. Chim. Acta* **1986**, *187*, 171–179. https://doi.org/https://doi.org/10.1016/S0003-2670(00)82910-4.

(112) Huber, P. J. Robust Estimation of a Location Parameter. *Ann. Math. Stat.* **1964**, *35* (1), 73–101. https://doi.org/10.1214/aoms/1177703732.

(113) Ortiz, M.; Sarabia, L.; Herrero, A. Robust Regression Techniques. A Useful Alternative for the Detection of Outlier Data in Chemical Analysis. *Talanta* **2006**, *70*, 499–512.

https://doi.org/10.1016/j.talanta.2005.12.058.

(114) Aguinis, H.; Gottfredson, R. K.; Joo, H. Best-Practice Recommendations for Defining, Identifying, and Handling Outliers. *Organ. Res. Methods* **2013**, *16* (2), 270–301. https://doi.org/10.1177/1094428112470848.

(115) Wada, K. Outliers in Official Statistics. *Japanese J. Stat. Data Sci.* **2020**, *3* (2), 669–691. https://doi.org/10.1007/s42081-020-00091-y.

(116) Rousseeuw, P. J.; Leroy, A. M. *Robust Regression and Outlier Detection*; Wiley Series in Probability and Statistics; Wiley, 2005.

(117) Speight, J. G. *Fuels for Fuel Cells*; Elsevier, 2011. https://doi.org/10.1016/B978-0-444-53563-4.10003-3.

(118) Montebelli, A.; Visconti, C. G.; Groppi, G.; Tronconi, E.; Ferreira, C.; Kohler, S. Enabling Small-Scale Methanol Synthesis Reactors through the Adoption of Highly Conductive Structured Catalysts. *Catal. Today* **2013**, *215*, 176–185. https://doi.org/https://doi.org/10.1016/j.cattod.2013.02.020.

(119) Yusup, S.; Phuong Anh, N.; Zabiri, H. A Simulation Study of an Industrial Methanol Reactor Based on Simplified Steady-State Model. *Ijrras* **2010**, *5* (3), 213–222.

(120) Masoudi, S.; Farsi, M.; Rahimpour, M. R. Dynamic Optimization of Methanol Synthesis Section in the Dual Type Configuration to Increase Methanol Production. *Oil Gas Sci. Technol.* **2019**, *74*. https://doi.org/10.2516/ogst/2019062.

(121) Meunier, N.; Chauvy, R.; Mouhoubi, S.; Thomas, D.; De Weireld, G. Alternative

Production of Methanol from Industrial CO2. *Renew. Energy* **2020**, *146*, 1192–1203. https://doi.org/10.1016/j.renene.2019.07.010.

(122) Terreni, J.; Borgschulte, A.; Hillestad, M.; Patterson, B. D. Understanding Catalysis—a Simplified Simulation of Catalytic Reactors for CO2 Reduction. *ChemEngineering* **2020**, *4* (4), 1–16. https://doi.org/10.3390/chemengineering4040062.

(123) Leonzio, G. Methanol Synthesis: Optimal Solution for a Better Efficiency of the Process. *Processes* **2018**, *6* (3). https://doi.org/10.3390/pr6030020.

(124) Pérez-Fortes, M.; Schöneberger, J. C.; Boulamanti, A.; Tzimas, E. Methanol Synthesis Using Captured CO2 as Raw Material: Techno-Economic and Environmental Assessment. *Appl. Energy* **2016**, *161*, 718–732. https://doi.org/10.1016/j.apenergy.2015.07.067.

(125) Oreggioni, G. D.; Brandani, S.; Luberti, M.; Baykan, Y.; Friedrich, D.; Ahn, H. CO2 Capture from Syngas by an Adsorption Process at a Biomass Gasification CHP Plant: Its Comparison with Amine-Based CO2 Capture. *Int. J. Greenh. Gas Control* **2015**, *35*, 71–81. https://doi.org/10.1016/j.ijggc.2015.01.008.

(126) Pröll, T.; Hofbauer, H. H2 Rich Syngas by Selective CO2 Removal from Biomass Gasification in a Dual Fluidized Bed System - Process Modelling Approach. *Fuel Process. Technol.* **2008**, *89* (11), 1207–1217. https://doi.org/10.1016/j.fuproc.2008.05.020.